ADVANCED FUNCTIONAL MATERIALS
www.afm-journal.de

Molecular Engineering of Blue Fluorescent Molecules Based on Silicon End-Capped Diphenylaminofluorene Derivatives for Efficient Organic Light-Emitting Materials

By *Kum Hee Lee, Lee Kyung Kang, Jin Yong Lee, Sunwoo Kang, Soon Ok Jeon, Kyoung Soo Yook, Jun Yeob Lee,** and *Seung Soo Yoon**

Blue fluorescent materials based on silicone end-capped 2-diphenylaminofluorene derivatives are synthesized and characterized. These materials are doped into a 2-methyl-9,10-*di*-[2-naphthyl]anthracene host as blue dopant materials in the emitting layer of organic light-emitting diode devices bearing a structure of ITO/DNTPD (60 nm)/NPB (30 nm)/emitting layer (30 nm)/Alq_3 (20 nm)/LiF (1.0 nm)/Al (200 nm). All devices exhibit highly efficient blue electroluminescence with high external quantum efficiencies (3.47%–7.34% at 20 mA cm^{-2}). The best luminous efficiency of 11.2 cd A^{-1} and highest quantum efficiency of 7.34% at 20 mA cm^{-2} are obtained in a device with CIE coordinates (0.15, 0.25). A deep-blue OLED with CIE coordinates (0.15, 0.14) exhibits a luminous efficiency of 3.70 cd A^{-1} and quantum efficiency of 3.47% at 20 mA cm^{-2}.

1. Introduction

In the past decade, organic light-emitting diodes (OLEDs) have attracted much scientific and commercial interest because of potential application in full-color displays and large-area, flexible, light-weight light sources.[1–4] Due to the requirements for full-color displays, many developments have been made in sets of the primary color emitters of red, green, and blue (RGB). Recently, most researches were focused on the development of blue-emitting materials as the design of blue materials with high efficiency, color purity, and long operation time was difficult due to the wide energy bandgap of blue materials.[5–11] It is well known that a dopant/host emitter system can significantly improve the device performances such as electroluminescence (EL) efficiency, emissive color, and operational lifetime.[1] Energy transfer from the host to the dopant was the main mechanism for the light emission in the host/dopant system and dopant emission was mainly observed. Various blue-emitting dopant materials have been developed, which include 4,4′-*bis*[2-(4-(*N*,*N*,-diphenylamino)phenyl)vinyl]-biphenyl (BDAVBi),[12] diphenylamino-di(styryl)arylene (DSA-Ph),[13] 4-[((*N*,*N*,-diphenylamino)phenyl)vinyl]-terphenyl,[14] and 9-ethyl-3-(4-phenylquinolin-2-yl)-9*H*-carbazole.[15] However, the efficiency, lifetime, and color chromaticity of the blue emitters should be further improved.

In this paper, the synthesis, characterization, and EL properties of new, highly efficient blue-light-emitting dopant materials is reported in detail. The blue dopant materials (**1–12**) were based on a 2-diphenylaminofluoren-7-yl-vinylarene core and various silicon-substituted end-capping groups (Scheme 1). In these dopant materials, the diphenylaminofluorene core was combined with a vinylarene unit to enhance the light-emitting efficiency by providing an extended conjugated structure and to obtain a deep-blue color from the fluorene unit's wide bandgap energy. The silicone end-capping groups could prevent intermolecular interaction of the dopant materials through steric hindrance of the nonplanar silicon moieties and reduce the self-quenching effect between dopant materials. Also, the role of the silicon moieties in forming thermally stable and pin-hole-free amorphous thin films was demonstrated.[16] Thereby, the silicon moieties would contribute to the high efficiency and deep-blue color of OLED devices even at high doping concentrations. Ten dopant materials (except for **3** and **4**) had various silicon end-capping groups on the diphenylaminofluorene-7-yl-vinylarene core unit to study systematically the effect of silicon moieties on the electroluminescent properties of the blue dopant materials. Four dopant materials (**1**, **2**, **5**, **6**) had the diphenylaminofluorene-7-yl-vinylfluorene core unit end-capped with triphenylsilylphenyl, trimethylsilylphenyl, trimethylsilyl, and triphenylsilyl groups. Five dopant materials (**7**, **8**, **9**, **10**, **11**) had end-capping groups such as 4-triphenylsilylphenyl,

[*] Prof. S. S. Yoon, Dr. K. H. Lee, L. K. Kang, Prof. J. Y. Lee, S. Kang
Department of Chemistry
Sungkyunkwan University
300 Cheoncheon-dong, Jangan-gu, Suwon, Gyeonggi, 440-746 (Korea)
E-mail: ssyoon@skku.edu
Prof. J. Y. Lee, S. O. Jeon, K. S. Yook
Department of Polymer Science and Engineering
Dankook University
126, Jukjeon-dong, Suji-gu, Yongin, Gyeonggi, 448-701 (Korea)
E-mail: leej17@dankook.ac.kr

DOI: 10.1002/adfm.200901895

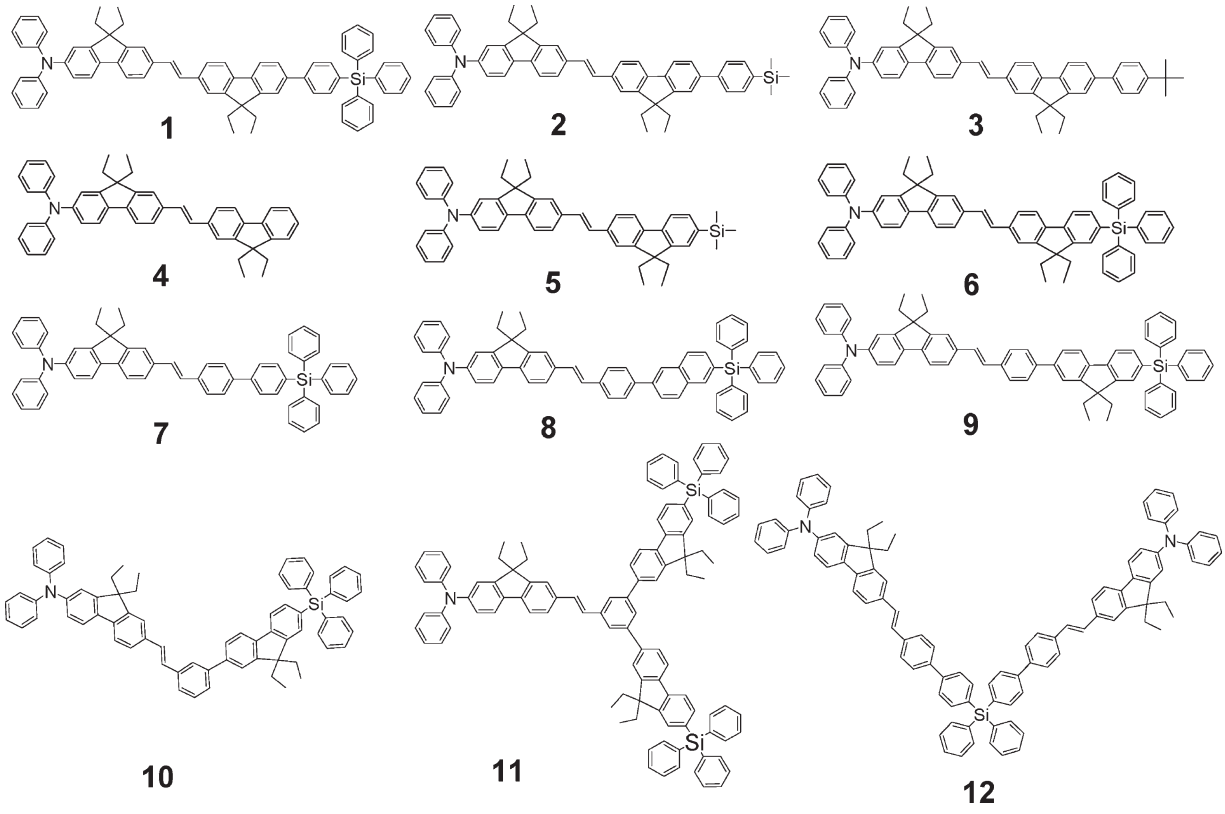

Scheme 1. Molecular structures of the blue fluorescent materials (**1**–**12**).

4-triphenylsilylnaphthyl, 4-triphenylsilylfluorenyl, 3-triphenylsilylfluorenyl, and 3,5-bis-triphenylsilylfluorenyl groups on the diphenylaminofluorene-7-yl-vinylphenyl core unit. Compound **12** had two diphenylaminofluorene-7-yl-vinylphenyl groups on the tetraphenylsilane unit. These various end-capping groups based on the silicon moieties in dopant materials played an important role in the EL performances of OLED devices through steric and electronic effects. As will be demonstrated below, the structural variations of the silicon end-capping groups in the blue dopant materials lead to significant difference in the device performances of the blue OLED devices.

2. Results and Discussion

2.1. Synthesis

The synthesis of the blue fluorescent materials (**1–12**) is outlined in Scheme 2. The aldehyde intermediates (**15**) were prepared by Suzuki coupling of bromo-aldehydes with the corresponding boronic acids or ester compounds (**14** and **25**). The Suzuki-cross coupling of formylphenylboronic acid with the corresponding bromo-intermediate afforded aldehyde intermediates such as **21**, **22**, **23**, and **26** in moderate to good yields. In addition, compound **7** was prepared by Suzuki reaction of 7-(4-dibromostryryl)-9,9-diethyl-*N*,*N*-diphenyl-fluorene-2-amine with triphenyl(4-(4,4,5,5-tetramethyl-1,3,2-dioxaborolan-2-yl)phenyl)silane. The monosilylation of 2,7-dibromo-9,9-diethylfluorene with chlorotrimethylsilane and chlorotriphenylsilane in the presence of n-BuLi in tetrahydrofuran (THF), and the subsequent formylation with dimethylformamide (DMF) in the presence of n-BuLi, afforded aldehyde intermediates (**18** and **19**). Formylation of 2-bromo-7-(diphenylamino)-9,9-diethylfluorene with DMF in the presence of n-BuLi in THF and the subsequent reduction with sodium borohydride in ethanol afforded the alcohol intermediate **28**. Michaelis–Arbuzov reaction of **28** with triethylphosphite in the presence of catalytic amounts of iodine afforded the phosphonate intermediate **29** in good yield. Finally, the Horner–Wadsworth–Emmons reaction between (7-(diphenylamino)-9,9-diethylfluorene-2-yl)methylphosphonate and the corresponding aldehyde afforded the blue-emitting materials (**1–6**, **8–12**) in moderate yields. After purification by column chromatography and recrystallization, these newly synthesized blue-emitting materials (**1–12**) were purified further by train sublimation at the reduced pressure below 10^{-3} torr and fully characterized with ^{1}H- and ^{13}C-NMR spectroscopy, IR spectroscopy, and low- and high-resolution mass spectrometry. High-pressure liquid chromatography (HPLC) analysis was carried out to check the purity of materials. These analyses revealed that the purity of blue-emitting materials (**1–12**) is at least above 99.0%.

2.2. Optical and Thermal Properties

UV-vis absorption and photoluminescent (PL) spectra of the blue materials (**1–12**) in dichloromethane are shown in

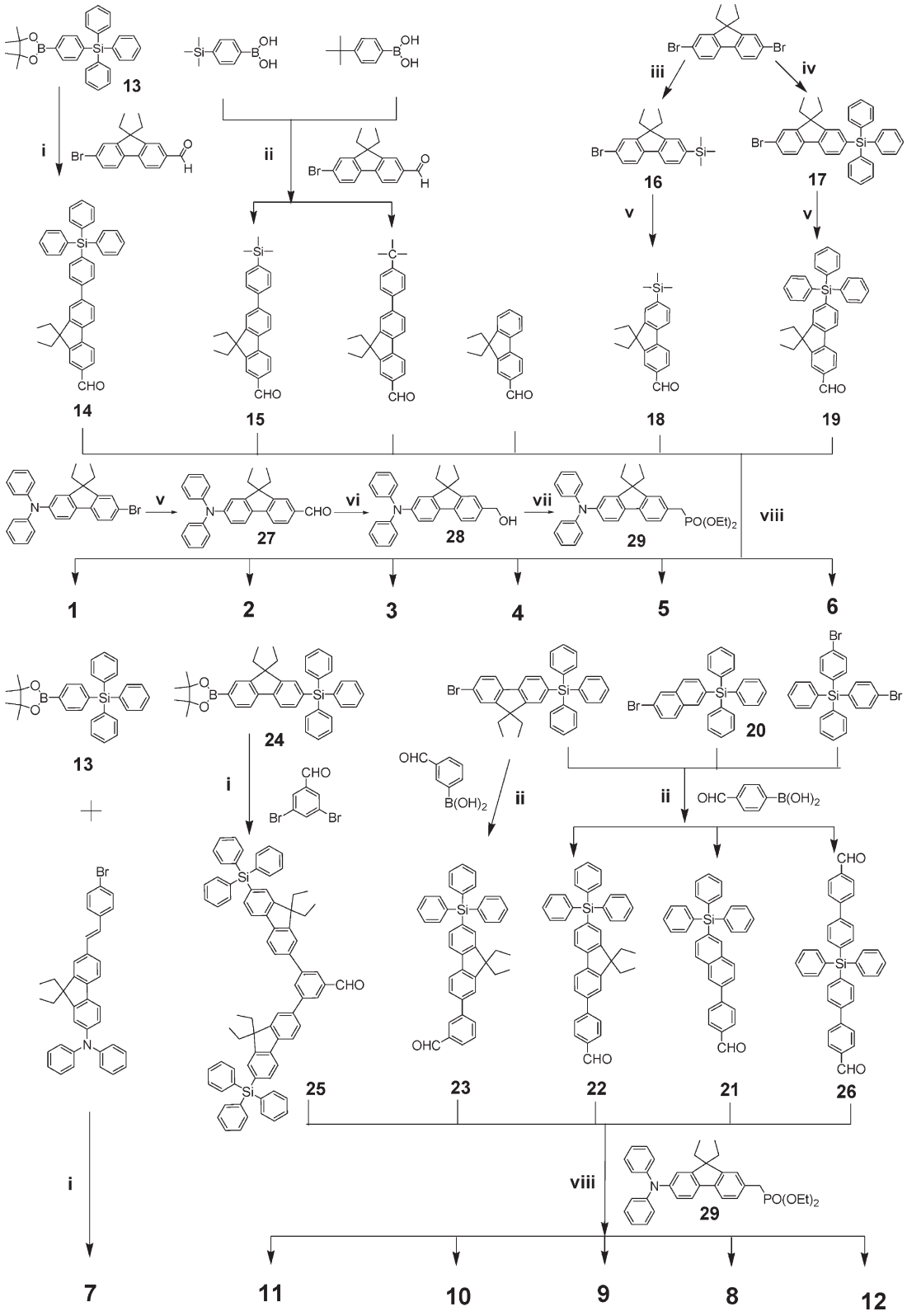

Scheme 2. Synthesis of the blue fluorescent materials (**1–12**). Reagents: i) $Pd(PPh_3)_4/Ka_2CO_3$/toluene/Aliquat 336; ii) $Pd(PPh_3)_4/Na_2CO_3$/toluene/EtOH; iii) n-BuLi/chlorotrimethylsilane /THF; iv) n-BuLi/chlorotriphenylsilane/THF; v) n-BuLi/DMF/THF; vi) $NaBH_4$/EtOH; vii) $I_2/P(OEt)_3$; viii) KO*t*-Bu/THF.

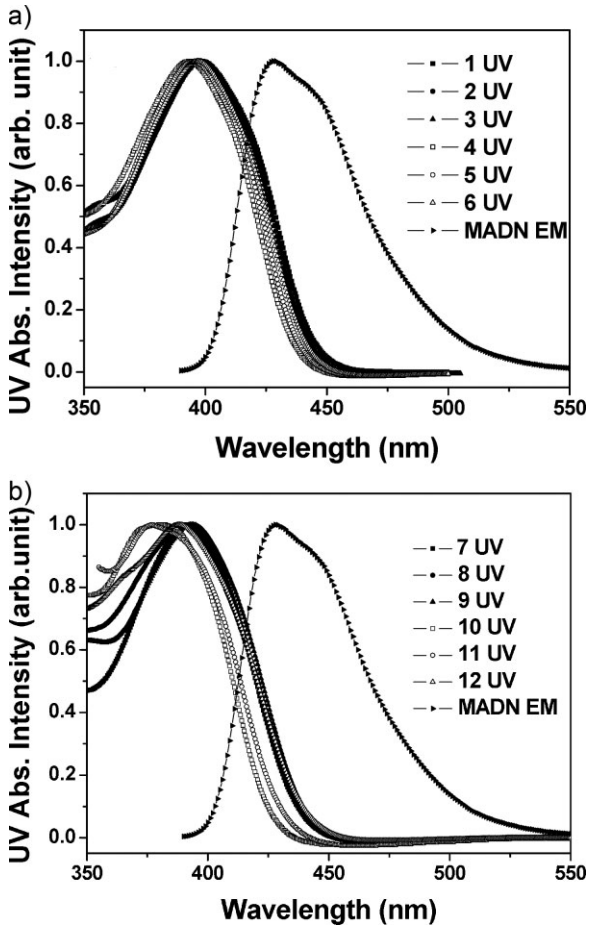

Figure 1. UV spectra of the blue fluorescent materials (**1–12**).

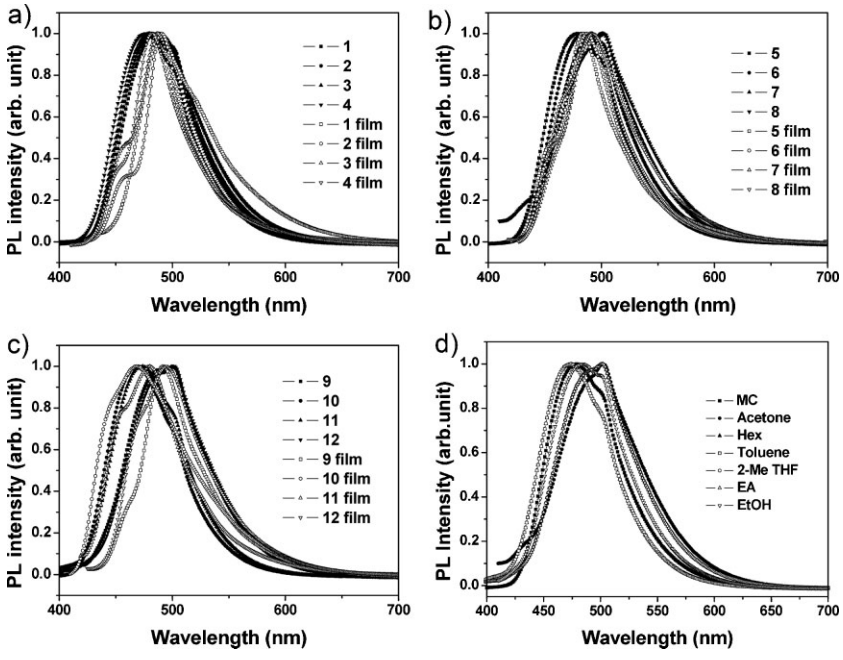

Figure 2. a–c) PL spectra of the blue fluorescent materials (**1–12**) in dichloromethane and solid thin film. d) PL spectra of the blue fluorescent material **5** in various solvents.

Figures 1 and 2, and the results summarized in Table 1. The PL emission spectrum of 2-methyl-9,10-*di*-[2-naphthyl]anthracene (MADN) with a maximum peak at 430 nm was well overlapped with the UV-vis absorption of the dopant materials. Therefore, efficient energy transfer from MADN to the blue fluorescent materials (**1–12**) through a Förster energy transfer was expected, indicating that MADN acts as a good host material in OLED devices using these materials (**1–12**) as dopants. The maximum emission peaks for **1–12** ranged from 468 to 502 nm in the blue region of the visible spectrum. As shown in Figure 2, compared the PL spectra of **4**, the PL spectra of the other materials were red-shifted in the order of **5**, **3**, **2**, **6**, and **1** due to the increase of π-conjugation of the end-capping groups in the dopant materials. PL spectra indicated that **10** and **11** were blue-shifted by approximately 31 and 27 nm, respectively, compared to **9** with the triphenylsilylfluorenyl end-capping group at the *para* position of diphenylaminofluoren-7-yl-vinylphenyl core unit, due to the incorporation of the same end-capping groups at the *meta* position that interrupt the π-conjugation between the core units and the end-capping groups. Interestingly, the maximum emission peak for **7** was similar to that of **12**, which had two fluorophores connected through a tetraphenylsilicon moiety. This observation indicates that the π-conjugation between two fluorophores through silicon moiety is not effective. Their full width at half maximum (FWHM) values ranged from 72 to 79 nm. The overall quantum yields of these materials were very high ($\Phi = 0.73$–0.86), suggesting that (**1–12**) might be good blue-emitting materials in OLED devices. To test the solvent effect on the PL spectra of these materials, the PL spectra of **5** in the various solvents were measured and are shown in Figure 2d. The maximum emission peaks for **5** in the various solvents varied from 474 to 502 nm. A red-shift is observed for solutions with an increasing polarity of solvent. This observation demonstrated the high sensitivity of the luminescence spectra of these materials to the solvent effect. The PL spectra of the blue materials (**1–12**) in thin solid film on quartz plates are appeared in Figure 2. The maximum emission peaks of **1–6**, **10**, and **11** in thin films were similar to those acquired in dilute solution, but with slight red-shifts (1–9 nm). These small spectra shifts in solid state spectra imply that the intermolecular interactions were weak because they were restrained effectively by the end-capped diphenylamino-fluorene groups. Intriguingly, **7–9** and **12** with 2-diphenylaminofluoren-7-yl-vinylphenyl cores end-capped with a triphenylsilyl group showed a maximum emission wavelength that was blue-shifted (6–10 nm) in thin film compared to the solution.

The solid PL data of **9** was measured according to doping concentration to confirm the energy transfer from the MADN host to the blue dopant materials. Figure 3 shows the solid PL spectra of the MADN film doped with dopant **9** according to doping concentration. The MADN film showed PL emission at 444 nm and the MADN emission disappeared in the MADN film doped with dopant **9**. This confirms the efficient energy transfer from the

Table 1. Physical properties of the compounds.

Dopant	UV λ_{max} [nm][a]	PL λ_{max} [nm] [a]/[b]	FWHM[nm] [a]/[b]	HOMO	LUMO	Bandgap	Φ_f[c]	T_g[°C]
1	398	487/489	78/69	−5.57	−2.67	2.81	0.77	109
2	398	482/491	75/42	−5.51	−2.71	2.82	0.81	105
3	397	480/487	73/49	−5.47	−2.73	2.83	0.86	109
4	393	476/482	73/48	−5.56	−2.70	2.86	0.88	82
5	395	479/484	73/55	−5.52	−2.67	2.85	0.90	86
6	396	485/487	75/54	−5.56	−2.73	2.83	0.84	107
7	391	500/491	78/58	−5.56	−2.64	2.83	0.83	104
8	390	502/492	77/76	−5.53	−2.76	2.86	0.78	113
9	393	500/492	78/55	−5.52	−2.68	2.84	0.73	120
10	380	468/469	72/87	−5.56	−2.64	2.92	0.85	109
11	377	473/480	72/71	−5.59	−2.69	2.90	0.85	144
12	388	501/495	79/74	−5.51	−2.67	2.84	0.47	143

[a] In CH_2Cl_2 (ca. 1×10^{-5} M). [b] Solid thin film on quartz plates. [c] Using BDAVBi as a standard; $\lambda_{ex} = 360$ nm ($\Phi = 0.86$ in CH_2Cl_2).

MADN host to the dopant materials. In addition, there was little red-shift of the PL emission even at high doping concentration, indicating little intermolecular interaction in the doped film.

The triphenylsilyl type blocking group also affects the thermal stabilities of the dopant materials and they are summarized in Table 1. Comparing dopants **4**, **5** and **6**, the glass transition temperature (T_g) of **6** with the triphenylsilyl group was increased by more than 20 °C compared with that of **4** without any end-capping group. The trimethylsilyl group slightly increased the T_g due to its small size. The other dopant materials with triphenylsilyl groups also showed high T_g over 100 °C, indicating that the tripheylsilyl end-capping group is effective to improve the thermal stability of the materials.

2.3. Morphological Stability

The morphological stability of the dopant materials with triphenylsilyl end-capping groups was studied. Figure 4 shows atomic force microscopic (AFM) images of the dopant materials. The surface roughness of the evaporated film of dopants **7** and **9** was around 0.3 nm. They formed a smooth film, indicating good morphological stability of the dopant materials. The triphenylsilyl end-capping group was helpful to form a stable morphology in the pure film.

2.4. HOMO-LUMO Energy Levels

The highest occupied molecular orbital (HOMO) energy levels of the dopant materials were estimated using an AC-2 photoelectron

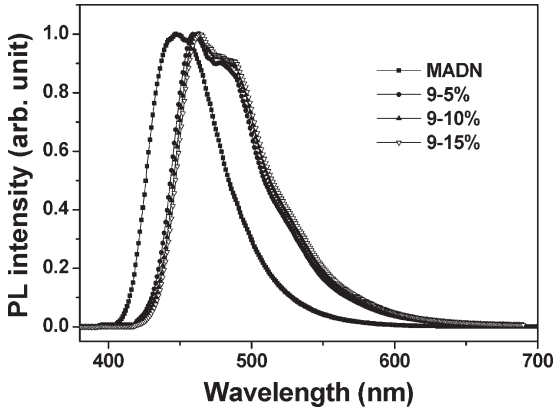

Figure 3. Solid PL spectra of the MADN doped with dopant **9** at doping concentrations of 5%, 10%, and 15%.

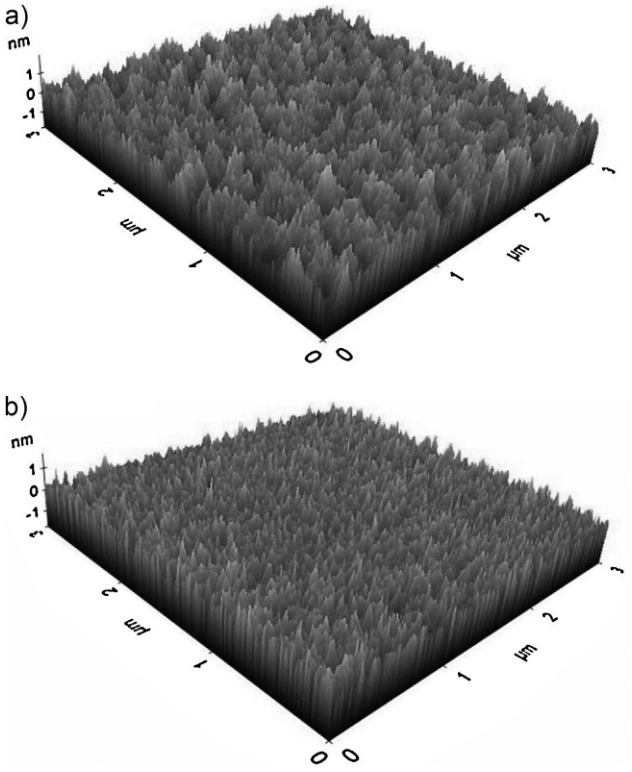

Figure 4. AFM topographic images (angled view) of a) material **7** film (Ra: 0.35 nm) and b) material **9** film (Ra: 0.32 nm). Ra = roughness average.

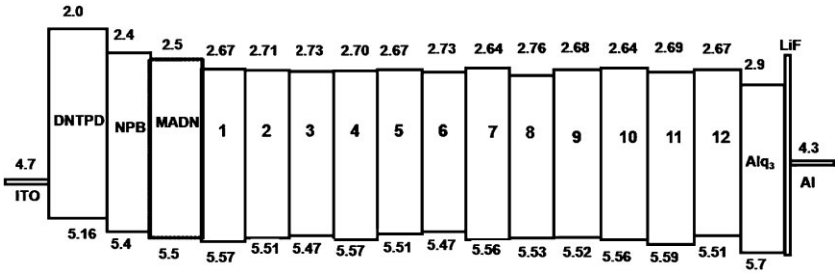

Figure 5. Energy levels of the materials used in the devices.

spectrometer. The HOMO energy levels for (**1–12**) varied from −5.47 to −5.59 eV (Table 1). The lowest unoccupied molecular orbital (LUMO) energy levels were calculated by subtracting the optical bandgap from the HOMO energy levels and they were between −2.64 and −2.76 eV. The bandgaps of the dopant materials (**1–12**) were ranged from 2.81 to 2.92 eV and they were narrower than that (3.0 eV) of a common blue host material, MADN. This implies that MADN can be a good host material for the dopant (**1–12**) materials. As the energy level difference between the MADN and the dopant materials was less than 0.2 eV, it is expected that charge trapping is not significant in the blue device doped with the dopant (**1–12**) materials. Figure 5 shows the HOMO and LUMO energy levels of blue fluorescent materials (**1–12**) along with other materials used in EL devices, including indium tin oxide (ITO), *N,N′*-diphenyl-*N,N′-bis*-[4-(phenyl-*m*-tolyl-amino)-phenyl]-biphenyl-4,4′-diamine (DNTPD), *N,N′*-di(1-naphthyl)-*N,N′*-diphenylbenzidine (NPB), MADN, *tris*(8-hydroxyquinoline) aluminium (Alq_3), and LiF/Al.

2.5. Quantum-Mechanical Calculation of Electronic Structure

Density functional theory (DFT) calculations for blue dopant materials (**1–12**) were carried out using a suite of Gaussian 03 program to understand the observed properties of the dopant materials at the molecular level. The nonlocal density functional of Becke's 3-parameters employing Lee-Yang-Parr functional (B3LYP) with 6-31G* basis sets was used for the calculation.[17]

The optimized structures and distributions of the HOMO and LUMO orbitals for blue dopant materials (**1–12**) are shown in Figure 6. The dihedral angles between fluorene (linked with

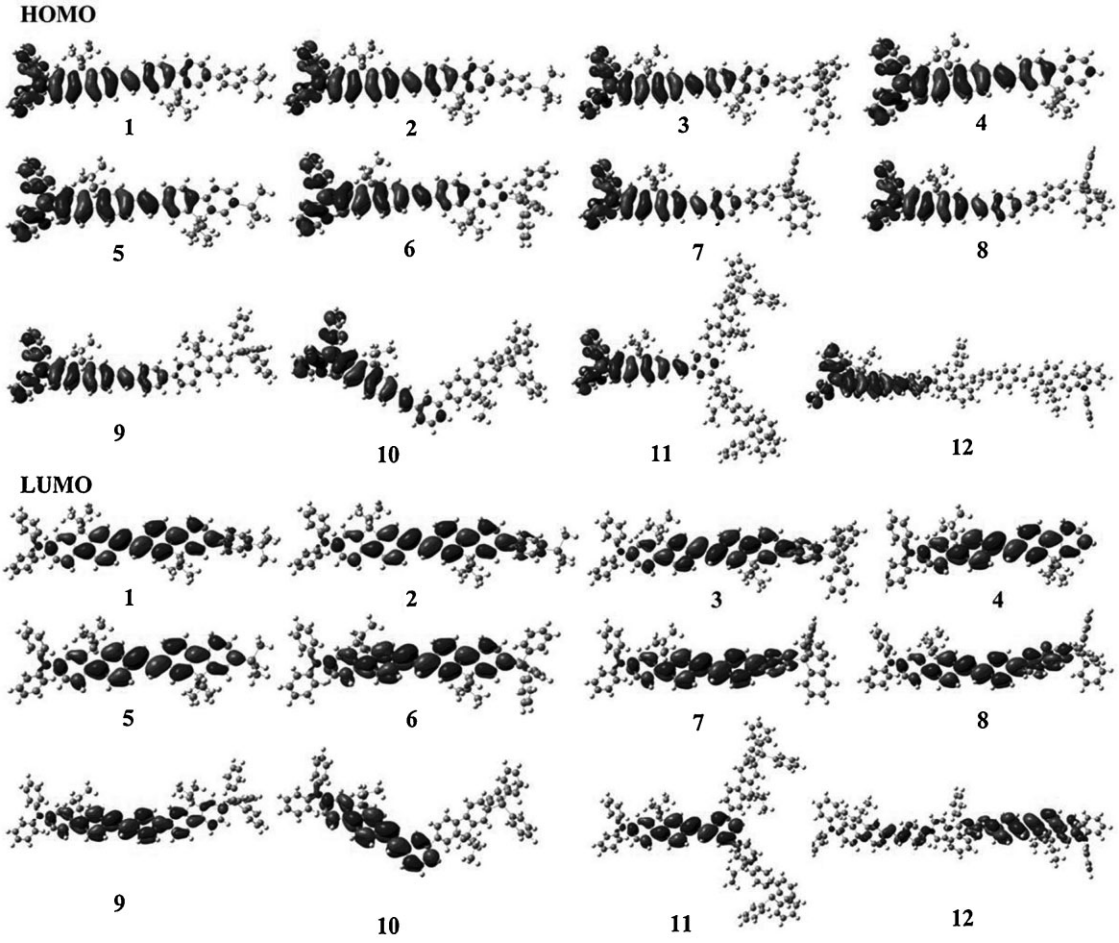

Figure 6. B3LYP/6-31G* calculated HOMOs and LUMOs of the blue fluorescent materials (**1–12**).

Table 2. Oscillator strength and electronic transition probability for compounds **1–12**.

Compound	1	2	3	4	5	6	7	8	9	10	11	12
Oscillation strength	1.9689	1.9428	1.9963	1.5386	1.6555	1.7232	1.5501	1.6051	1.9027	1.2905	1.9070	1.3802
Electronic oscillators	100%	100%	100%	100%	100%	100%	100%	100%	100%	100%	100%	100%

diphenyl amine) and fluorene for **1–6** were calculated to be 2.04, 5.03, 5.04, 20.3, 20.5, and 21.6, respectively. For **7–11**, the dihedral angles between the fluorene (linked with diphenyl amine) and phenyl moieties were calculated to be 3.0, 1.1, 7.3, 16.1, and 3.06, respectively. In the case of **12**, the left and right side dihedral angles between the fluorene and phenyl moieties were calculated to be 3.01 and 12.35, respectively.

Molecules can absorb light and undergo a transition from one molecular orbital state to another molecular state. The oscillation strength is a dimensionless quantity to expresses the strength of transition, and it gives relative transition probability. The oscillation strength f_{ij} of a transition from a lower molecular orbital state to an upper molecular orbital state may be defined by $f_{ij} = 2m_e/3\hbar^2 (E_j - E_i) \sum_n \sum_\alpha |<\psi_j|R_{n,\alpha}|\psi_i>|^2$, where E_i and ψ_i are the energy and the wavefunction of the ith state, m_e is the electron mass, $R_{n,\alpha}$ is the atomic position with atomic index n and $\alpha = x, y, z$, and $\hbar = h/2\pi$, where h is the planck constant. To obtain the excitation energies and oscillator strength (transition probability) and to compare with the experimental transition properties, the time-dependent DFT (TDDFT) calculations were carried out at the optimized geometries. It was found that the electronic transition with the highest oscillator strength was the transition from the HOMO to LUMO, for all compounds listed in Table 2. The excitation energies for blue dopant materials (**1–12**) were calculated to be 2.7679, 2.7789, 2.7923, 2.7679, 2.8609, 2.8349, 2.8196, 2.8339, 2.7918, 2.7972, 2.9533, 2.9136, and 2.8063 eV, respectively, that correspond to the respective absorption wavelengths: 447.94, 446.17, 444.02, 433.38, 437.35, 439.73, 437.50, 444.10, 443.24, 419.81, 425.54, and 441.81 nm. These values are in good agreement with the experimental bandgaps and absorption wavelengths.

2.6. EL Properties

Blue devices with a structure ITO/DNTPD (60 nm)/NPB (30 nm)/ *x*% dopant:MADN (30 nm)/Alq_3 (20 nm)/LiF(1.0 nm)/Al (200 nm) were fabricated to explore the EL properties of the dopant materials. The doping concentration of the dopant materials was controlled from 5% to 15% to study the concentration quenching effect. The device performances of the dopant materials are summarized in Table 3 and the EL spectra of the blue devices with 10% doping concentration (**A2–L2**) are shown in Figure 7. Two EL peaks were observed for **A2–I2** and **K2**, whereas **J2** and **L2** had only one emission peak. The EL spectra of the doped blue devices were similar to PL spectra of the corresponding dopant materials. No MADN emission was observed because of the effective energy transfer from the MADN to the dopant material as explained in Figure 3. The blue devices doped with the dopant materials showed superior EL performances compared with that of the MADN device without any doping. Compared with the device C2 doped with the dopant **3** with a *t*-butylphenyl end-capping group, the device B2 doped with dopant **2** with a trimethylsilylphenyl end-capping group showed blue-shifted CIE coordinates due to the steric and electronic effects of the nonplanar silicon moieties. The red-shift of the emission color of **E2** and **F2** compared to **D2** originates from the silicon effects of the dopant materials by trimethylsilane and triphenylsilane moieties. The blue-shift of the emission color of the **J2** and **K2** devices compared to **I2** is in good agreement with the PL spectra.

The EL spectra of devices **J** and **L** were monitored according to the doping concentration to study the effect of end-capping group on the EL spectra of the blue devices. The EL spectra of **J** and **L** at 8 V are depicted in Figure 7c. There was little change of the EL spectra even at a high doping concentration of 15%, indicating that intermolecular interaction between dopant molecules was suppressed in the **J** and **L** devices. In the case of the device **C** and **D** doped with the dopant without the end-capping group, the red-shift of the emission spectrum was observed as shown in the color index data in Table 3. The color index of devices **J2** and **L2** were essentially little changed according to doping concentration. The nonplanar end-capping groups with silicon moieties effectively prevented the dopant aggregation at high doping concentration, resulting in stable color index according to doping concentration.

Current density–voltage–luminance (*I–V–L*) measurements of the blue devices were performed under ambient conditions and the results are summarized in Table 3. *I–V–L* characteristic of devices (**A1–A3**) and the efficiency versus current density relationship of devices **A2**, **F2**, and **I2** are shown in Figure 8. The current density and luminance of device **A** were increased at high doping concentration. The charge trapping effect is not significant in the MADN:dopant **1** structure because there is less than 0.2 eV energy level difference. Therefore, the increase of the current density of **A3** with high doping concentration is due to the good hole-transport properties of dopant **1**. The dopant materials contribute to the charge transport at high doping concentration because the dopant materials synthesized in this work have the aromatic amine moiety with good hole-transport properties. The amine group may improve the hole-transport properties of the emitting layer. This was confirmed in the device current density–voltage data of the blue device at high doping concentration of 50% and 100%. Although it is not shown here, the current density was increased at high doping concentration and the highest current density was obtained in the device with only dopant as the emitting material without any MADN. The improved hole injection was further confirmed in the hole-only and electron-only device data of the MADN doped with the dopant material. The hole current density was much higher than the electron current density, showing that the dopant improves the hole transport in the emitting layer.

Intriguingly, the device performance for **J2** was poor, suggesting that the topological structure of the core unit led to drastic differences in performances of the solid-state devices. With the exception of device **J2**, all devices showed high external quantum

Table 3. EL properties of devices **A–L**.

Device	Dopant [wt%]	Luminance L [cd m^{-2}][a]	η_{ext} [%][b]	η_L [cd A^{-1}][b]	η_P [lm W^{-1}][b]	$V_{turn\text{-}on}$ [V]	λ_{max} [nm] [c]
MADN		1297 (10)	1.96	2.40	1.28	6.0	462 (0.15, 0.16)
A1	**1** (5%)	26650 (10)	6.90	10.2	4.43	5.0	460, 487 (0.15, 0.23)
A2	**1** (10%)	25690 (10)	7.34	11.2	4.87	5.5	461, 488 (0.15, 0.25)
A3	**1** (15%)	35500 (10)	7.13	10.8	5.00	5.0	462, 488 (0.15, 0.24)
B1	**2** (5%)	23450 (9.0)	7.15	9.45	4.69	4.5	458, 483 (0.15, 0.19)
B2	**2** (10%)	17940 (9.0)	5.96	8.75	4.78	4.5	461, 485 (0.15, 0.22)
B3	**2** (15%)	27990 (9.0)	5.76	8.58	4.58	4.5	461, 486 (0.15, 0.23)
C1	**3** (5%)	18430 (9.0)	6.23	8.79	4.36	4.5	459, 484 (0.15, 0.21)
C2	**3** (10%)	21240 (9.0)	4.51	6.94	3.44	4.5	461, 485 (0.15, 0.24)
C3	**3** (15%)	26290 (9.0)	3.58	5.89	3.15	4.5	462, 487 (0.15, 0.26)
D1	**4** (5%)	25160 (9.5)	5.67	6.78	3.14	4.5	452, 479 (0.15, 0.17)
D2	**4** (10%)	9943 (9.0)	3.84	4.95	2.46	4.5	453, 477 (0.15, 0.19)
D3	**4** (15%)	10420 (9.0)	3.84	5.46	2.71	4.0	454, 479 (0.15, 0.19)
E1	**5** (5%)	18920 (9.0)	6.60	8.24	4.09	5.0	455, 478 (0.15, 0.18)
E2	**5** (10%)	14810 (9.0)	5.16	6.95	3.45	5.5	456, 481 (0.15, 0.20)
E3	**5** (15%)	19040 (9.0)	4.71	6.67	3.31	4.5	457, 481 (0.15, 0.21)
F1	**6** (5%)	19310 (9.0)	7.35	9.79	4.86	4.5	458, 481 (0.15, 0.20)
F2	**6** (10%)	20200 (9.0)	7.08	9.89	4.91	4.5	460, 483 (0.15, 0.21)
F3	**6** (15%)	21120 (9.0)	6.80	9.62	4.78	4.5	460, 483 (0.15, 0.22)
G1	**7** (5%)	13330 (9.5)	5.63	7.43	3.44	5.5	458, 479 (0.15, 0.19)
G2	**7** (10%)	14220 (9.5)	6.18	8.54	3.95	5.5	460, 481 (0.15, 0.21)
G3	**7** (15%)	15590 (9.5)	6.34	9.12	4.23	5.0	463, 482 (0.15, 0.22)
H1	**8** (5%)	15390 (9.5)	5.39	6.72	3.59	4.5	458, 480 (0.15, 0.17)
H2	**8** (10%)	19130 (9.0)	6.24	8.37	4.15	5.0	460, 481 (0.15, 0.20)
H3	**8** (15%)	25880 (9.0)	5.51	7.49	4.00	4.5	461, 480 (0.15, 0.20)
I1	**9** (5%)	15170 (9.5)	6.00	8.52	3.95	5.5	462, 483 (0.15, 0.22)
I2	**9** (10%)	16120 (9.5)	6.46	9.74	4.51	5.5	462, 486 (0.15, 0.24)
I3	**9** (15%)	23900 (9.5)	6.66	10.1	4.66	5.5	463, 485 (0.15, 0.24)
J1	**10** (5%)	7125 (8.5)	2.99	3.19	1.71	4.5	456 (0.15, 0.14)
J2	**10** (10%)	10500 (9.0)	3.47	3.70	1.98	5.0	456 (0.15, 0.14)
J3	**10** (15%)	7021 (8.5)	3.00	3.40	1.82	4.5	456 (0.16, 0.15)
K1	**11** (5%)	11090 (8.5)	4.97	6.01	3.21	5.0	457, 481 (0.15, 0.16)
K2	**11** (10%)	17040 (9.0)	6.03	7.83	3.89	5.5	459, 485 (0.15, 0.19)
K3	**11** (15%)	25330 (10.)	5.08	7.22	3.34	5.0	459, 485 (0.15, 0.21)
L1	**12** (5%)	18290 (10)	4.96	9.02	3.92	5.5	487 (0.17, 0.31)
L2	**12** (10%)	21780 (9.5)	5.21	9.37	4.34	5.5	479 (0.17, 0.31)
L3	**12** (15%)	17740 (9.5)	4.61	8.32	3.86	5.0	477 (0.17, 0.31)

[a] Maximum luminance. Values in parentheses are the voltages at which the maximum values were obtained. [b] Values collected at 20 mA cm^{-2}. [c] Values collected at 8 V and CIE coordinates (x,y) are shown in parentheses.

efficiencies (EQE) greater than 4.51%, with little efficiency roll-off within the current density investigated as shown in Table 3. In addition, the molecular structure of the blue dopant materials can be correlated with the device performances. First of all, the silicon end-capping groups improved greatly the EL properties of the blue OLED devices. For example, the comparison of the EQE of device **D2** (3.84%) and device **E2** (5.16%) shows that the addition of the trimethylsilyl end-capping group in the blue dopant material increases the device EQE by 46%. Furthermore, the change of the end-capping group from trimethylsilyl to triphenylsilyl increased the EQE by 37% (**E2** versus **F2**). These observations indicated that the substituents of dopant materials such as the trimethylsilane and triphenylsilane moieties played an important role of improving the EL performances of the devices. In addition, the comparison of the EQE of **B2** (5.96%) and **C2** (4.51%) showed that the replacement of the *t*-butyl end-capping group with the trimethylsilyl group increased the device EQE by 30%. Furthermore, the change in end-capping groups from trimethylsilyl to triphenylsilyl increased the EQE by 23% (**A2** versus **B2**). The emitting cores of dopant materials **1**, **2**, **5**, and **6** were protected by the bulky trimethylsilane and triphenylsilane substituents, respectively, and the intermolecular interaction between dopant materials was greatly suppressed. The reduced molecular aggregation prevented the self-quenching between dopant materials and improved the EL performances. In comparison with devices **A2** and **B2**, the EQE of devices **F2** and **E2** was improved by 13% and 16%, respectively. Interestingly, the introduction of a phenyl ring to the same core structure of dopant material improved the device performances of the blue devices. In particular, device **A2** exhibited a much better performance, yielding an EQE of 7.34% and a luminous efficiency of 11.2 cdA^{-1} at 20 mA cm^{-2}.

Other blue dopant materials such as **7**, **8**, **9**, **11**, and **12** with triphenylsilyl end-capping groups showed high EQEs (from 5.21%

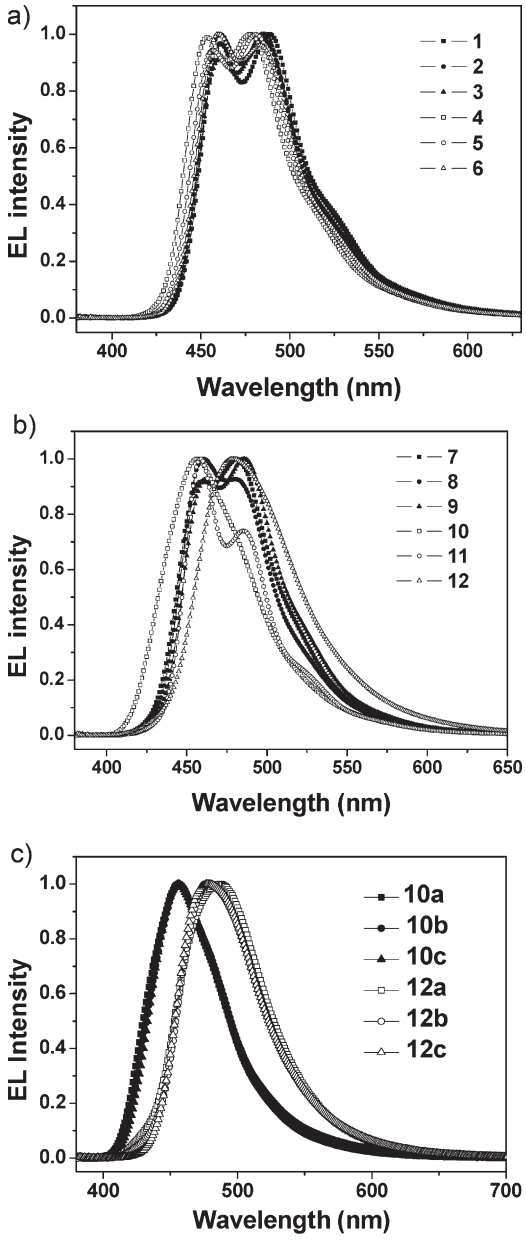

Figure 7. EL spectra of devices (**A2–L2**).

to 6.46%) that nearly exceeded the theoretical limit of fluorescent OLEDs.[18–20] Among those, blue material **12** had interesting structural features, two 2-diphenylaminofluoren-7-yl-vinylphenyl cores bridged with a diphenylsilyl group, while material **7** has one 2-diphenylaminofluoren-7-yl-vinylphenyl core end-capped with a triphenylsilyl group. However, the device performance of **L2** was not superior to those of the **G2**. Although the luminous and power efficiencies of device **L2** were higher than those of **G2**, the EQE of **L2** was lower than that of **G2**. This low EQE of device **L2** may be attributed to the low quantum yield of the dopant material **12**.

The device performances of the blue OLEDs could be correlated with the position of the triphenylsilyl end-capping groups. When the triphenylsilylfluorenyl end-capping group on the 2-diphenylaminofluoren-7-yl-vinylphenyl core structure changed from the *para* to the *meta* position, the EQE decreased 46% from 6.46% to 3.47% in devices **I2** and **J2**. Furthermore, it was found that the introduction of another triphenylsilylfluorenyl end-capping group at the *meta* position of the core structure increased the EQE by 74% from 3.47% to 6.03% (**J2** and **K2**). These efficiency changes may be partially attributed to the differences in effectiveness of exciton formation on dopant materials through energy transfer between the MADN host material and the dopant materials within devices **I2**, **J2**, and **K2**, because the quantum yields of dopant materials (**9–11**) are in a similar range, 0.73 to 0.85. The degree of overlap between dopant material emission and MADN host material absorption increases in order of dopant materials **10**, **11**, and **9**, as shown in Figure 1. These observations imply that effectiveness of exciton formation on dopant materials through energy transfer between the MADN host material and dopant materials increased in the same order. Thus, the improved efficiencies in the order of devices **J2**, **K2**, and **I2** indicate that the effective energy transfer between host and dopant would play an important role in the highly efficient blue OLEDs. The device performances of the dopant materials **1** and **6–9** were respectively high in this work. Therefore, further development of the analogous derivatives of the dopant materials can afford materials with improved properties.

The dependence of the quantum efficiency on doping concentration could also be correlated with the molecular structure of the dopant materials. The efficiency was optimized at low doping concentration in the devices without any blocking group, while the efficiency was optimized to a relatively high doping concentration in the devices with the bulky blocking group. A serious self-quenching effect was observed in devices **C** and **D** because no end-capping group was introduced. In the cases of **B** and **E**, a similar self-quenching effect was observed because the trimethylsilyl group is not bulky enough to isolate the emitting core structure. Therefore, a similar self-quenching effect was observed. The degree of efficiency decrease in devices **B**, **C**, **D**, and **E** was significant at 15% compared with that of other devices with bulky triphenylsilyl groups. The efficiency of the devices was maximized at 5% doping concentration. In the case of **F**, even though a maximum efficiency was observed at 5%, there was less than 10% decrease of the efficiency and the color shift was also not significant because the self-quenching of the dopant was reduced due to the bulky triphenylsilyl capping group. In other devices, the optimum doping concentration was 10% or 15% because of the triphenylsily end-capping group, which can suppress the self-quenching effect. In the cases of **G** and **I**, the efficiency was a little further improved at 15%, but the degree of improvement was not so significant. Therefore, it can be said that the triphenylsilyl group suppresses the self-quenching effect and the blue device could show high efficiency at high doping concentration compared with the blue device doped with blue dopants without any blocking group.

Lifetime data of the blue devices are shown in Figure 9. The lifetime of the blue devices was measured at a constant luminance of 1 000 cd m^{-2}. The lifetime of the blue dopant materials with the same core and different end-capping group was compared. The device **F2** with the triphenylsilyl end-capping group was better than devices **C2**, **D2**, and **E2** without or with trimethylsilyl end-capping group. The improved thermal stability and morphological stability of dopant **6** may improve the lifetime of the device. In addition the

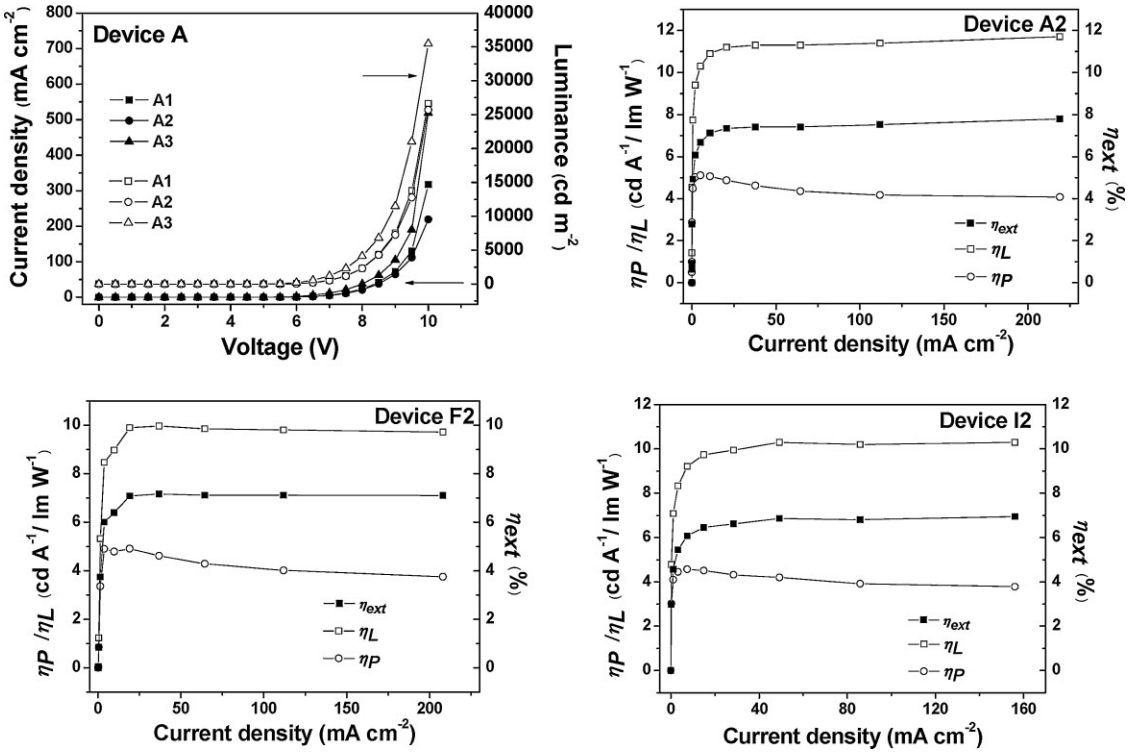

Figure 8. *I–V–L* characteristics of devices (**A1–A3**) (closed symbols: current density; closed symbols: luminance) and the efficiency versus current density relationship for devices **A2**, **F2**, and **I2**.

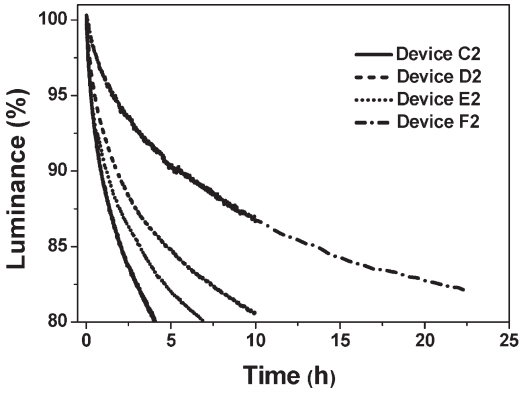

Figure 9. Device operational stability for devices **C2**, **D2**, **E2**, and **F2**.

high efficiency of the dopant material **6** compared with **3**, **4**, and **5** may also be responsible for the long lifetime.

3. Conclusions

A series of blue fluorescent dopant materials, 2-diphenylamino-fluorene derivatives end-capped with various silicon substituent units, were synthesized by the Horner–Wadsworth–Emmons and Suzuki reactions. The use of these blue fluorescent materials as dopants in OLED devices significantly improved the luminous efficiency and EQEs of OLED performance due to the steric effect of silicon end-capping groups that prevented molecular aggregation and self-quenching of the dopant materials in the devices. The best luminous efficiency of 11.2 cd A^{-1} and highest quantum efficiency of 7.34% at 20 mA cm^{-2} was obtained in a device using fluorescent material **1** as a dopant with CIE coordinates (0.15, 0.25). Also, a deep-blue OLED using dopant material **10** with CIE coordinates (0.15, 0.14) exhibited a luminous efficiency of 3.70 cd A^{-1} and quantum efficiency of 3.47% at 20 mA cm^{-2}. These studies clearly demonstrate the excellent properties of dopant materials containing silicon moieties for application in blue-emitting materials in OLEDs.

4. Experimental

General Information: All reactions were performed under nitrogen. Solvents were carefully dried and distilled from appropriate drying agents prior to use. Commercially available reagents were used without further purification unless otherwise stated. 7-Bromo-9,9-diethylfluorene-2-carboxaldehyde [21], 4-bromophenyl-triphenylsilane [22], 9,9-diethyl-fluorene-2-carbaldehyde [23], 2,7-dibromo-9,9-diethylfluorene [24], tetraphenylsilane dibromide [25], and (7-bromo-9,9-diethylfluoren-2-yl)diphenylamine[26] were prepared according to literature methods. ^{1}H- and ^{13}C-NMR spectra were recorded using a Varian (Unity Inova 300Nb) spectrometer at 300 MHz. FT-IR spectra were recorded using a VERTEX 70 spectrometer. Low- and high-resolution mass spectra were recorded using either a Jeol JMS-AX505WA spectrometer in FAB mode or a Jeol JMS-600 spectrometer in EI mode. HPLC were obtained on a Younglin SDV 50A instrument using a Shiseido C18 column, eluted with MeOH/EtOAc 9:1 (v/v).

General Procedure for the Horner–Wadsworth–Emmons Reaction: To a solution of (7-(diphenylamino)-9,9-diethyl-fluorene-2-yl)-methylphosphonate (1.5 mmol) and corresponding aldehyde (1.5 mmol) in THF in an ice

bath, potassium-*tert*-butoxide (2.3 mmol) was added under nitrogen. The reaction mixture was stirred for 15 min at 0 °C, followed by 1 h at room temperature, and quenched with water. The solution mixture was extracted with ethyl acetate and washed twice with water. The combined organic layers were dried over $MgSO_4$ and the solvent removed under reduced pressure to afford a crude product that was purified by column chromatography with silica gel and subsequent recrystallization from CH_2Cl_2/MeOH.

Compound Characterization: **1** (68% Yield): ^{1}H-NMR (300 MHz, $CDCl_3$, δ): 7.71 (t, J = 7.0 Hz, 3H), 7.68 (d, J = 5.8 Hz, 5H), 7.62 (d, J = 8.3 Hz, 9H), 7.53 (d, J = 8.2 Hz, 4H), 7.48 (s, 2H), 7.41 (d, J = 8.2 Hz, 7H), 7.28–7.23 (m, 4H), 7.14–7.11 (d, J = 8.8 Hz, 6H), 7.05–6.98 (m, 4H), 2.10–1.88 (m, 8H), 0.38 (t, J = 7.0 Hz,12H); ^{13}C-NMR (75 MHz, $CDCl_3$, δ): 151.8, 151.1, 151.0, 150.6, 148.3, 147.4, 142.9, 141.4, 141.1, 141.0, 139.9, 137.2, 136.9, 136.7, 136.0, 134.5, 133.0, 129.9, 129.4, 128.9, 128.4, 128.2, 126.8, 126.4, 126.1, 126.0, 124.1, 123.9, 122.7, 121.8, 120.9, 120.8, 120.6, 120.3, 120.2, 119.6, 56.4, 56.3, 33.2, 33.0, 30.0, 25.1, 8.9, 1.3; IR (KBr): 3016, 2969, 1738, 1365, 1282, 1216, 1017, 755, 731 cm^{-1}; FABMS (m/z): 970 [M^+ + H]; HRMS (FAB, m/z): [M^+ + H] calcd for $C_{72}H_{64}NSi$, 970.4884; found, 970.4816; mp 253 °C.

2 (50% Yield): ^{1}H-NMR (300 MHz, $CDCl_3$, δ): 7.78 (d, J = 8.0 Hz, 4H), 7.69–7.66 (m, 7H), 7.64–7.58 (m, 6H), 7.57 (d, J = 7.3 Hz, 6H), 7.25 (s, 5H), 2.24–1.99 (m, 8H), 0.39–0.20 (m, 12H); ^{13}C-NMR (75 MHz, $CDCl_3$, δ): 152.7, 151.9, 151.9, 151.5, 149.2, 148.3, 143.2, 142.2, 141.9, 141.8, 141.1, 140.2, 137.7, 137.6, 136.9, 134.9, 130.3, 129.7, 129.3, 127.7, 127.2, 127.0, 126.9, 124.9, 124.8, 123.6, 122.7, 121.8, 121.7, 121.5, 121.1, 121.0, 120.5, 57.3, 57.2, 34.1, 33.9, 0.10; IR (KBr): 2961, 1564, 1493, 1467, 1275, 1248, 841, 813, 696 cm^{-1}; FABMS (m/z): 783 [M^+]; HRMS (FAB, m/z): [M^+] calcd for $C_{57}H_{57}NSi$, 783.42601; found, 783.4255; mp 183 °C.

3 (58% Yield): ^{1}H-NMR (300 MHz, $CDCl_3$, δ): 7.73 (t, J = 7.0 Hz, 4H), 7.64–7.56 (m, 10H), 7.51 (t, J = 8.8 Hz, 4H), 7.13 (d, J = 7.3 Hz, 2H), 7.04–6.98 (m, 8H), 2.11–1.89 (m, 8H), 0.49–0.36 (m, 21H); ^{13}C-NMR (75 MHz, $CDCl_3$, δ): 152.7, 151.9, 151.8, 151.5, 151.3, 149.5, 148.3, 142.2, 141.4, 141.0, 137.6, 130.3, 129.7, 129.4, 127.9, 127.0, 126.9, 1245.0, 124.8, 123.6, 122.6, 121.7, 121.6, 121.4, 121.0, 120.5, 57.2, 57.1, 35.6, 34.1, 33.9, 32.5, 9.73; IR (KBr): 2969, 1739, 1590, 1493, 1468, 1273, 816, 747, 697 cm^{-1}; FABMS (m/z): 767 [M^+]; HRMS (FAB$^+$, m/z): [M^+] calcd for $C_{58}H_{57}N$, 767.4491; found, 767.4500; mp 219 °C.

4 (32% Yield): ^{1}H-NMR (300 MHz, $CDCl_3$, δ): 7.69 (d, J = 8.8 Hz, 2H), 7.59–7.33 (m, 7H), 7.30 (d, J = 13.5 Hz, 5H), 7.12 (d, J = 8.8 Hz, 6H), 7.05–6.98 (m, 5H), 2.13–1.88 (m, 8H), 0.41–0.32 (m, 12H); ^{13}C-NMR (75 MHz, $CDCl_3$, δ): 151.9, 150.7, 150.5, 148.4, 147.5, 141.6, 141.5, 141.4, 136.9, 136.8, 136.1, 129.5, 128.9, 128.6, 127.3, 127.2, 126.2, 126.0, 124.2, 124.0, 123.2, 122.8, 120.9, 120.8, 120.7, 120.2, 119.9, 119.7, 119.6, 56.4, 33.2, 33.1, 8.9, 8.8; IR (KBr): 3024, 2961, 2920, 1587, 1460, 1277, 956, 744 cm^{-1}; FABMS (m/z): 635 [M^+]; HRMS (FAB, m/z): [M^+] calcd for $C_{48}H_{45}N$, 635.3552; found, 635.3557; mp 133 °C.

5 (45% Yield): ^{1}H-NMR (300 MHz, $CDCl_3$, δ): 7.68 (d, J = 7.6 Hz, 1H), 7.70 (d, J = 8.2 Hz, 1H), 7.62–7.45 (m, 8H), 7.5 (t, J = 8.3 Hz, 6H), 7.13 (d, J = 8.2 Hz, 5H), 7.05–6.99 (m, 3H), 2.10–1.90 (m, 8H), 0.41–0.31 (m, 21H); ^{13}C-NMR (75 MHz, $CDCl_3$, δ): 151.9, 151.0, 150.7, 149.6, 148.4, 147.5, 142.2, 141.5, 141.4, 139.4, 137.0, 136.1, 132.3, 129.5, 128.9, 128.6, 127.8, 126.2, 126.0, 124.2, 124.0,122.8, 121.0, 120.8, 120.7, 120.3, 119.7,119.6, 119.3, 56.4, 56.3, 33.1, 9.0, 8.9; IR (ATR): 3020, 2957, 1585, 1481, 1276, 954, 823, 747,692 cm^{-1}; FABMS (m/z): 707 [M^+]; HRMS(FAB, m/z): [M^+] calcd for $C_{51}H_{53}NSi$, 707.3947; found, 707.3947; mp 207 °C.

6 (40% Yield): ^{1}H-NMR (300 MHz, $CDCl_3$, δ): 7.71 (d, J = 8.8 Hz, 1H), 7.70 (d, J = 7.0 Hz, 1H), 7.61 (dd, J = 8.2, 1.8 Hz, 6H), 7.57–7.51 (m, 6H), 7.48 (s, 3H), 7.47–7.42 (m, 3H), 7.40 (d, J = 8.2 Hz, 5H), 7.37–7.36 (m, 7H), 7.14–7.10 (m, 4H), 7.05–6.99 (m, 3H), 2.04–1.02 (m, 8H), 0.41–0.34 (t, J = 6.7 Hz, 12H); ^{13}C-NMR (75 MHz, $CDCl_3$, δ): 151.9, 151.0, 150.7, 149.6, 148.3, 147.5, 142.2, 141.5, 141.4, 139.4, 137.0, 136.8, 136.1, 130.1, 132.3, 129.8, 129.7, 129.5, 128.9, 128.6, 127.8, 126.2, 126.0, 124.4, 124.2, 124.0, 122.8, 121.0, 120.8, 120.7, 120.3, 119.7, 119.6, 119.2, 56.7, 56.3, 33.1, 9.0, 8.9, 0.5; IR (KBr): 3028, 2962, 2919, 1588, 1480, 1275, 1105, 743, 699 cm^{-1}; FABMS (m/z): 893 [M^+]; HRMS(FAB, m/z): [M^+] calcd for $C_{66}H_{59}NSi$, 893.4417; found, 893.4409; mp 239 °C.

8 (68% Yield): ^{1}H-NMR (300 MHz, $CDCl_3$, δ): 8.09 (d, J = 6.5 Hz, 2H), 7.87 (t, J = 7.0 Hz, 2H), 7.80 (s, 1H), 7.79–7.69 (m, 4H), 7.68–7.61 (m, 9H), 7.55 (t, J = 8.8 Hz, 3H), 7.50–7.44 (m, 7H), 7.42 (d, J = 7.63 Hz, 4H), 7.14–7.12 (dd, J = 1.17 Hz, 7.0 Hz, 6H), 7.06–6.99 (m, 5H), 2.03–1.91 (m, 4H), 0.83 (t, J = 6.6 Hz, 6H); ^{13}C-NMR (75 MHz, $CDCl_3$, δ): 151.9, 150.7, 148.3, 147.5, 141.6, 140.0, 139.2, 137.7, 137.2, 136.7, 136.6, 135.8, 134.5, 134.4, 132.8, 132.3, 132.2, 123.0, 129.8, 129.5, 129.2, 128.2, 127.9, 127.7, 127.3, 127.2, 126.3, 125.7, 125.6, 124.1, 123.9, 122.8, 120.9, 120.7, 119.6, 56.3, 33.0, 8.9; IR (KBr): 3025, 2970, 1738, 1488, 1467, 1428, 1109, 817, 743, 698 cm^{-1}; FABMS (m/z): 875 [M^+]; HRMS (FAB, m/z): [M^+] calcd for $C_{62}H_{51}N$, 875.3947; found, 875.3933; mp 117 °C.

9 (70% Yield): ^{1}H-NMR (300 MHz, $CDCl_3$, δ): 7.74 (d, J = 8.8 Hz, 2H), 7.70 (d, J = 7.7 Hz, 3H), 7.85–7.65 (m, 10H), 7.54 (d, J = 7.6 Hz, 4H), 7.48–7.39 (m, 11H), 7.22 (d, J = 8.8 Hz,4H), 7.13 (d, J = 8.8 Hz, 5H), 7.05–6.99 (m, 4H), 2.01–1.85 (m, 8H), 0.38 (t, J = 7.3 Hz, 12H); ^{13}C-NMR (75 MHz, $CDCl_3$, δ): 151.9, 151.4, 150.7, 149.6, 148.3, 147.5, 142.9, 141.5, 140.9, 140.7, 140.3, 136.9, 136.7, 135.8, 135.6, 134.9, 132.7, 131.1, 130.8, 129.8, 129.6, 129.4, 128.1, 127.6, 127.4, 127.1, 126.2, 126.1, 124.1, 123.9, 122.8, 121.5, 120.8, 120.6, 119.6, 56.4, 56.31, 33.0, 32.9, 8.9; IR (KBr): 2969, 1739, 1590, 1488, 1466, 1428, 1110, 814 cm^{-1}; FABMS (m/z): 969 [M^+]; HRMS (FAB, m/z): [M^+] calcd for $C_{72}H_{63}NSi$, 969.4730; found, 969.4733; mp 237 °C.

10 (40% Yield): ^{1}H-NMR (300 MHz, $CDCl_3$, δ): 7.82–7.34 (m, 4H), 7.64–7.53 (m, 17H), 7.50–7.45 (d, J = 7.0 Hz, 8H), 7.43–7.42 (d, J = 7.1 Hz, 8H), 7.14–7.10 (d, J = 6.8 Hz, 6H), 2.10−2.00 (m, 8H), 0.38 (t, J = 7.1 Hz, 12H); ^{13}C-NMR (75 MHz, $CDCl_3$, δ): 151.9, 151.4, 150.7, 149.6, 148.3, 147.5, 142.9, 141.6, 140.9, 140.8, 138.4, 136.7, 136.7, 135.8, 135.6, 124.9, 132.7, 131.1, 130.0, 129.9, 129.5, 128.2, 127.8, 126.7, 126.4, 126.3, 125.7, 125.4, 124.1, 123.9, 122.8, 121.9, 120.7, 120.6, 119.6, 56.5, 56.3, 33.0, 32.9, 8.9, 8.9; IR (KBr): 3025, 2970, 1738, 1366, 1228, 1109, 697 cm^{-1}; FABMS (m/z): 969 [M^+]; HRMS (FAB, m/z): [M^+] calcd for $C_{72}H_{63}NSi$, 969.4730; found, 969.4708; mp 107 °C.

11 (88% Yield): ^{1}H-NMR (300 MHz, $CDCl_3$, δ): 7.85-7.70 (m, 21H), 7.62 (d, J = 7.0 Hz, 9H), 7.46–7.37 (m, 17H), 7.11 (d, J = 7.0 Hz, 6H), 7.06–6.99(m, 10H), 2.09–1.93 (m, 12H), 0.49 (t, J = 6.5 Hz, 18H); ^{13}C-NMR (75 MHz, $CDCl_3$, δ): 152.0, 151.5, 150.8, 149.7, 148.3, 147.6, 143.0, 142.9, 141.7, 141.1, 141.0, 139.0, 136.8, 135.8, 135.7, 134.9, 132.9, 131.2, 130.5, 129.9, 129.5, 128.2, 127.8, 126.7, 126.4, 124.6, 124.2, 124.0, 122.9, 122.2, 121.0, 120.7, 119.7, 56.6, 56.4, 33.1, 33.0, 9.0, 8.9; IR (KBr): 3025, 2970, 1738, 1366, 1277, 1228, 1216, 1109, 1003, 698 cm^{-1}; FABMS (m/z):1148 [M^+]; HRMS (FAB, m/z): [M^+] calcd for $C_{107}H_{93}NSi_2$, 1447.6847; found, 1447.6810; mp 139 °C.

12 (60% Yield): ^{1}H-NMR (300 MHz, $CDCl_3$, δ): 7.68–7.63 (m, 21H), 7.46–7.42 (m, 19H), 7.14 (d, J = 7.0 Hz, 12H), 7.03–7.01 (m, 10H), 2.02–1.88 (m, 8H), 0.40–0.33 (m, 12H); ^{13}C-NMR (75 MHz, $CDCl_3$, δ): 192.1, 151.9, 150.7, 148.3, 147. 2, 142.0, 141.6, 139.9, 137.5, 137.4, 137.2, 136.7, 135.8, 134.5, 133.3, 130.6, 130.1, 130.0, 129,8, 129.5, 128.8, 128.3, 128.3, 128.0, 127.6, 127.3, 127.3, 127.2, 127.1, 127.0, 126.3 124.1, 124.0, 123.9, 122.8, 122.7, 121.0, 120.9, 120.7, 120.6, 119.8, 119.6, 62.5, 62.4, 56.3, 33.0, 32.9, 16.7, 16.6, 8.9, 8.8; IR (KBr): 3025, 2971, 1738, 1490, 1466, 1366, 1029, 815, 753, 721 cm^{-1}; FABMS (m/z):1315 [M^+ + H]; HRMS (FAB, m/z): [M^+ + H] calcd for $C_{98}H_{83}N_2Si$, 1315.6326; found, 1315.6335; mp 125 °C.

General Procedure for the Suzuki Reaction, Synthesis of 7: Into a 50-mL, 2-necked round-bottomed flask containing 7-(4-bromostyryl)-9,9-diethyl-*N*,*N*-diphenyl-9H-fluoren-2-amine (342 mg, 0.6 mmol), triphenyl(4-(4,4,5,5-tetramethyl-1,3,2-dioxaborolan-2-yl)phenyl)silane (333 mg, 0.72 mmol), and tetrakis(triphenylphosphine)palladium(0) (28 mg, 0.024 mmol) was added toluene (10.0 mL). To this was added a solution of K_2CO_3 (0.83 mL of 2.0 M) and Aliquat 336 (0.03 mL, 0.06 mmol) dropwise. After the reaction mixture was refluxed at 120 °C for 3 h, the solution mixture was extracted with ethyl acetate and washed with water. The combined organic layer was dried with anhydrous Na_2SO_4, filtered, and evaporated to dryness. The crude product was purified by column chromatography with silica gel using ethyl acetate/hexane (1:20 v/v), affording a yellow solid with a yield of 280 mg (56%). ^{1}H-NMR (300 MHz, $CDCl_3$, δ): 7.62 (t, J = 7.0 Hz, 7H), 7.50–7.36 (m, 10H), 7.28–7.19 (m, 11H), 7.12 (d, J = 5.8 Hz, 5H), 7.05–6.98 (m, 8H), 2.04–1.85 (m, 4H), 0.38 (t, J = 6.5 Hz, 6H); ^{13}C-NMR (75 MHz, $CDCl_3$, δ): 152.8,

151.6, 149.1, 148.4, 142.8, 142.4, 140.8, 138.1, 137.6, 136.6, 135.3, 130.8, 130.7, 130.3, 129.1, 128.5, 128.2, 128.0, 127.4, 127.1, 125.0, 124.8, 123.6, 121.7, 121.5, 120.4, 57.2, 33.9, 9.7; IR (KBr): 3025, 2970, 1738, 1593, 1487, 1466, 1428, 1281, 1110, 816, 698 cm^{-1}; FABMS (*m/z*): 825 [M^+]; HRMS (FAB, *m/z*): [M^+] calcd for$C_{61}H_{51}NSi$, 825.3791; found, 825.3795; mp 139 °C.

Triphenyl(4-(4,4,5,5-tetramethyl-1,3-dioxolan-2-yl)phenyl)silane (13): To (4-bromophenyl)triphenylsilane (800 mg, 1.92 mmol) in anhydrous THF (10.0 mL) was added n-BuLi (1.8 mL of a 1.6 M solution in hexane, 2.88 mmol) within 30 min at −78 °C. After an additional hour, 2-isopropoxy-4,4,5,5,-tetramethyl-1,3,2-dioxaborolane (0.58 mL, 2.88 mmol) was added and the reaction mixture and allowed to warm to room temperature. Water was then added, followed by the usual extractive workup with ethyl acetate. The combined organic layers were dried with anhydrous $MgSO_4$, filtered, and evaporated to dryness. The crude product was purified by column chromatography with silica gel using ethyl acetate/hexane (1:20 v/v), affording a white solid white at a yield of 635 mg (81%). ^{1}H-NMR (300 MHz, $CDCl_3$, δ): 7.80 (d, J = 8.2 Hz, 2H), 7.57 (t, J = 8.2 Hz, 8H), 7.45–7.40 (m, 2H), 7.38–7.34 (m, 3H), 1.34 (s, 12H); ^{13}C-NMR (75 MHz, $CDCl_3$, δ): 138.0, 136.7, 135.9, 134.3, 134.1, 129.9, 128.1, 84.1, 25.1; IR (KBr): 3015, 2970, 1738, 1362, 1228, 1217, 1074, 998, 707 cm^{-1}; FABMS (*m/z*): 463 [M^+ + H]; HRMS (FAB, *m/z*): [M^+ + H] calcd for $C_{30}H_{32}BO_2Si$, 463.2265; found, 463.2265.

9,9-Diethyl-7-(4-(triphenylsilyl)phenyl)-9H-fluorene-2-carbaldehyde (14): **14** was prepared by the same procedure as for **7**, from triphenyl(4-(4,4,5,5-tetramethyl-1,3-dioxolan-2-yl)phenyl)silane (842 mg, 1.82 mmol) and (7-bromo-9,9-diethyl-9H-fluorene-2-carbaldehyde (500 mg, 1.52 mmol). Yield: 521 mg, 61%. ^{1}H-NMR (300 MHz, $CDCl_3$, δ): 10.06 (s, 1H), 7.87–7.86 (m, 4H), 7.69–7.60 (m, 10H), 7.55 (d, J = 6.5 Hz, 2H), 7.46–7.43 (m, 2H), 7.41 (d, J = 7.4 Hz, 4H), 7.39–7.36 (m, 3H), 2.15−2.08 (m, 4H), 0.34 (t, J = 7.0 Hz, 6H); ^{13}C-NMR (75 MHz, $CDCl_3$, δ): 192.6, 152.3, 151.3, 147.8, 142.4, 141.8, 139.7, 137.3, 136.7, 136.0, 135.6, 134.4, 134.2, 133.7, 131.0, 130.0, 128.2, 128.2, 126.9, 126.7, 123.4, 122.1, 121.6, 120.3, 56.7, 33.0, 25.1, 8.8; IR (KBr): 3015, 2970, 1738, 1366, 1229, 1216, 1111, 812, 698 cm^{-1}; FABMS (*m/z*): 585 [M^+ + H]; HRMS (FAB, *m/z*): [M^+ + H] calcd for $C_{42}H_{37}OSi$, 585.2614; found, 585.2611.

9,9-Diethyl-7-(4-(trimethylsilyl)phenyl)-9H-fluorene-2-carbaldehyde (15): **15** was prepared by the same procedure as for **21**, from 4-(trimethylsilylphenyl) boronic acid (354 mg, 1.82 mmol) and (7-bromo-9,9-diethyl-9H-fluorene-2-carbaldehyde (500 mg, 1.52 mmol). Yield: 454 mg, 75%. ^{1}H-NMR (300 MHz, $CDCl_3$, δ): 10.07 (s, 1H), 7.89–7.83 (m, 3H), 7.68–7.59 (m, 5H), 7.59 (s, 1H), 2.13−2.10 (m, 4H), 0.39–0.32 (m, 15H); ^{13}C-NMR (75 MHz, $CDCl_3$, δ): 152.8, 150.5, 142.1, 140.8, 140.5, 140.1, 139.6, 134.2, 130.4, 126.8, 126.6, 126.5, 121.9, 121.4, 56.8, 33.0, 8.8 0.8; IR (KBr): 3016, 2970, 1700, 1630, 1454, 1366, 1217, 778 cm^{-1}; FABMS (*m/z*): 399 [M^+ + H]; HRMS (FAB, *m/z*): [M^+ + H] calcd for $C_{27}H_{31}OSi$, 399.2144; found, 399.2138.

(7-Bromo-9,9-diethyl-9H-fluorene-2-yl)trimethylsilane (16): To 2,7-dibromo-9,9-diethylfluorene (1.50 g, 3.94 mmol) in anhydrous THF (50 mL) was added n-BuLi (2.71 mL of a 1.6 M solution in hexane, 4.34 mmol) within 30 min at −78 °C. After an additional hour, chlorotrimethylsilane (0.554 mL, 4.34 mmol) was added. The reaction mixture was then allowed to warm to room temperature and was quenched with water. The solution mixture was extracted with ethyl acetate and washed twice with water. The combined organic layer was dried with anhydrous $MgSO_4$, filtered, and evaporated to dryness. The crude product was purified by column chromatography with silica gel using ethyl acetate/hexane (1:10 v/v) to afford a pale yellow oil (1.30 g) at a yield of 88%. ^{1}H-NMR (300 MHz, $CDCl_3$, δ): 7.65 (d, J = 8.2 Hz, 1H), 7.56 (d, J = 8.8 Hz, 1H), 7.49 (dd, J = 7.0, 1.8 Hz, 1H), 7.46–7.43 (m, 3H), 2.03−2.00 (m, 4H), 0.37–0.29 (m, 15H); ^{13}C-NMR (75 MHz, $CDCl_3$, δ): 153.2, 149.4, 141.8, 141.3, 140.5, 132.9, 132.7, 130.8, 128.4, 128.3, 127.1, 121.9, 119.9, 57.1, 33.4, 9.5, 9.4, 0.1; IR (ATR): 3020, 2961, 2918, 1451, 1248, 839, 811, 751, 625 cm^{-1}; FABMS (*m/z*): 372 [M^+]; HRMS (FAB, *m/z*): [M^+] calcd for $C_{20}H_{25}{}^{79}$BrSi, 372.0909; found, 372.0901.

(7-Bromo-9,9-diethyl-9H-fluorene-2-yl)triphenylsilane (17): Compound **17** was synthesized similarly to compound **16** and was obtained (0.57 g) at a yield of 72%. ^{1}H-NMR (300 MHz, $CDCl_3$, δ): 7.64–7.61 (m, 3H), 7.59 (dd, J = 8.2, 1.5 Hz, 3H), 7.54 (s, 1H), 7.51 (d, J = 8.5 Hz, 2H), 7.47–7.44 (m, 4H), 7.43–7.41 (t, J = 4.1 Hz, 2H), 7.40 (d, J = 7.3 Hz, 6H), 1.97–1.89 (m, 4H), 0.33 (t, J = 7.2 Hz, 6H); ^{13}C-NMR (75 MHz, $CDCl_3$, δ): 153.0, 149.0, 142.2, 140.6, 136.7, 135.9, 135.7, 134.8, 134.8, 133.4, 131.1, 130.4, 130.3, 129.9, 128.2, 128.1, 126.7, 121.8, 121.7, 119.6, 64.0, 56.7, 35.0, 32.8, 19.3,14.2, 8.8; IR (ATR): 3057, 2961, 2921, 1106, 699, 505 cm^{-1}; FABMS (*m/z*): 558 [M^+]; HRMS (FAB, *m/z*): [M^+] calcd for $C_{35}H_{31}{}^{79}$BrSi, 558.1378; found, 558.1368.

9,9-Diethyl-7-(trimethylsilyl)-9H-fluorene-2-carbaldehyde (18): To **16** (0.86 g, 2.3 mmol) in anhydrous THF (13 mL) was added n-BuLi (2.2 mL of a 1.6 M solution in hexane, 3.45 mmol) within 30 min at −78 °C. The reaction mixture was stirred for 1 h before 0.28 mL (3.68 mmol) of DMF was added dropwise. After stirring for 1 h at −78 °C, the mixture was contained in an ice bath and treated with dilute hydrochloric acid (5.0 mL of 1.0 M). The organic phase was washed with water, aqueous sodium bicarbonate, and saturated sodium chloride solution. The combined organic layer was dried with anhydrous $MgSO_4$. After filtration and evaporation of the solvent, the crude product was purified by column chromatography with silica gel using hexanes/ethyl acetate (30:1 v/v) to give the desired compound as a bright green solid (0.65 g) at a yield of 87%. ^{1}H-NMR (300 MHz, $CDCl_3$, δ): 10.06 (s, 1H), 7.86 (d, J = 5.9 Hz, 3H), 7.76 (d, J = 7.0 Hz, 1H), 7.54(d, J = 7.6 Hz, 1H), 7.49 (s, 1H), 2.12−2.05 (m, 4H), 0.34–0.29 (m, 15H); ^{13}C-NMR (75 MHz, $CDCl_3$, δ): 192.6, 151.2, 150.7, 148.3, 141.9, 140.8, 135.7, 132.5, 130.8, 128.0, 123.5, 120.4, 120.3, 56.5, 32.8, 8.8, 0.6; IR (ATR): 3403, 2960, 2922, 1690, 1605, 1249, 831, 751 cm^{-1}; FABMS (*m/z*): 323 [M^+ + H]; HRMS (FAB, *m/z*): [M^+ + H] calcd for $C_{21}H_{27}OSi$, 323.1831; found, 323.1827.

9,9-Diethyl-7-(triphenylsilyl)-9H-fluorene-2-carbaldehyde (19): Compound **19** was synthesized similarly to compound **18** and obtained (0.57 g) at a yield of 72%. ^{1}H-NMR (300 MHz, $CDCl_3$, δ): 10.06 (s, 1H), 7.87 (s, 3H), 7.78 (d, J = 7.8 Hz, 1H), 7.59 (d, J = 6.9 Hz, 8H), 7.48–7.33 (m, 9H), 2.06–1.95 (m, 4H), 0.32 (t, J = 7.4 Hz, 6H); ^{13}C-NMR (75 MHz, $CDCl_3$, δ): 192.7, 151.5, 150.7, 148.0, 141.6, 136.7, 136.0, 135.8, 135.3, 134.5, 131.4, 130.8, 130.0, 128.3, 123.6, 120.7, 130.6, 56.6, 32.2, 8.8; IR (ATR): 3435, 2921, 1637, 1383, 1102, 753, 703, 703 cm^{-1}; FABMS (*m/z*): 509 [M^+ + H]; HRMS (FAB, *m/z*): [M^+ + H] calcd for $C_{36}H_{33}OSi$, 509.2301; found, 509.2300.

(6-Bromonaphthalen-2-yl)triphenylsilane (20): To 2,6-dibromonaphthalene (1.00 g, 3.49 mmol) in anhydrous THF (150 mL) was added n-BuLi (2.62 mL of a 1.6 M solution in hexane, 4.19 mmol) within 30 min at −78 °C. After an additional hour, triphenylsilylchloride (1.18 g, 4.02 mmol) was added and the reaction mixture and allowed to warm to room temperature. Water was then added, followed by the usual extractive workup with ethyl acetate. The combined organic layers were dried with anhydrous $MgSO_4$, filtered, and evaporated to dryness. The crude product was purified by column chromatography with silica gel using hexane, affording a white solid white at a yield of 730 mg (45%). ^{1}H-NMR (300 MHz, $CDCl_3$, δ): 8.04 (s, 1H), 7.78–7.68 (m, 1H), 7.464–7.61 (m, H), 7.56–7.39 (m, H); ^{13}C-NMR (75 MHz, $CDCl_3$, δ): 137.8, 136.8, 135.8, 135.3, 134.3, 133.5, 133.0, 131.6, 130.4, 130.3, 130.2, 130.1, 129.7, 128.4, 128.2, 128.1, 126.5, 126.4, 121.3; IR (KBr): 3015, 2970, 1738, 1427, 1366, 1228, 1216, 1108, 688 cm^{-1}; FABMS (*m/z*): 464 [M^+]; HRMS (FAB, *m/z*): [M^+] calcd for $C_{28}H_{21}{}^{79}$BrSi, 464.0596; found; 464.0585.

4-(6-(Triphenylsilyl)naphthalen-2-yl)benzaldehyde (21): To a 50-mL, 2-necked round-bottomed flask containing (6-bromonaphthalen-2-yl)triphenylsilane (752 mg, 1.62 mmol), 4-formylphenylboronic acid (291 mg, 1.94 mmol), and tetrakis(triphenylphosphine)palladium(0) (74.9 mg, 0.06 mmol) was added toluene (17.0 mL), EtOH (7.5 mL), and a solution of Na_2CO_3 (7.5 mL of 2.0 M) stepwise. After the reaction mixture was at 120 °C for 3 h, the solution mixture was extracted with ethyl acetate and washed with water. The combined organic layers were dried with anhydrous Na_2SO_4, filtered, and evaporated to dryness. The crude product was purified by column chromatography with silica gel using ethyl acetate/hexane (1:15 v/v), affording a light white solid at a yield of 680 mg (88%). ^{1}H-NMR (300 MHz, $CDCl_3$, δ): 10.1 (s, 1H), 8.10 (d, J = 7.6 Hz, 2H), 7.99 (d, J = 7.6 Hz, 2H), 7.87 (d, J = 7.6 Hz, 4H), 7.76–7.69 (m, 3H), 7.64–7.61 (m, 5H), 7.49–7.37 (m, 9H); ^{13}C-NMR (75 MHz, $CDCl_3$, δ): 192.2, 147.2, 138.1, 137.7, 136.7, 135.5, 134.3, 134.3, 133.3, 133.1, 132.8, 130.6, 130.0,

129.6, 128.3, 128.2, 127.8, 126.7, 125.5; IR (KBr): 3015, 2970, 1738, 1484, 1366, 1314, 1217, 1110, 744, 682 cm^{-1}; FABMS (*m/z*): 491 [$M^+ + H$]; HRMS (FAB, *m/z*): [$M^+ + H$] calcd for $C_{35}H_{27}OSi$, 491.1831; found, 491.1842.

4-(9,9-Diethyl-7-(triphenylsilyl)-9H-fluoren-2-yl)benzaldehyde (22): **22** was prepared by the same procedure as for **21**, from (7-bromo-9,9-diethyl-9H-fluoren-2-yl)triphenylsilane (1.60 g, 2.86 mmol) and 4-formylphenylboronic acid (514 mg, 3.43 mmol). Yield: 1.10 g, 75%. ^{1}H-NMR (300 MHz, $CDCl_3$, δ): 10.01 (s, 1H), 8.09 (s, 1H), 7.87 (d, $J = 8.8$ Hz, 1H), 7.85 (d, $J = 8.3$ Hz, 1H), 7.81 (d, $J = 8.0$ Hz, 1H), 7.69 (d, $J = 7.0$ Hz, 1H), 7.63–7.57 (m, 11H), 7.47–7.35 (m, 9H), 2.02–1.95 (m, 4H), 0.36–0.30(t, $J = 7.0$ Hz, 6H); ^{13}C-NMR (75 MHz, $CDCl_3$, δ): 192.8, 151.6, 149.6, 1428, 142.56, 141.6, 139.2, 137.2, 136.7, 1356, 134.8, 133.4, 133.1, 131.1, 129.9, 129.7, 129.0, 128.3, 128.1, 126.4, 121.8, 120.7, 119.7, 56.5, 32.9, 8.9; IR (KBr): 3015, 2970, 1738, 1703, 1427, 1366, 1228, 1216, 1140, 1085, 681 cm^{-1}; FABMS (*m/z*): 584 [M^+]; HRMS (FAB, *m/z*): [M^+] calcd for $C_{42}H_{36}OSi$, 584.2535; found, 584.2543.

3-(9,9-Diethyl-7-(triphenylsilyl)-9H-fluoren-2-yl)benzaldehyde (23): **23** was prepared by the same procedure as for **21**, from (7-bromo-9,9-diethyl-9H-fluoren-2-yl)triphenylsilane (850 mg, 1.52 mmol) and 3-formylphenylboronic acid (273 mg, 1.82 mmol). Yield: 650 mg, 84%. ^{1}H-NMR (300 MHz, $CDCl_3$, δ): 10.11 (s, 1H), 8.17 (s, 1H), 7.93 (d, $J = 8.8$ Hz, 1H), 7.85 (d, $J = 8.3$ Hz, 1H), 7.81 (d, $J = 8.0$ Hz, 1H), 7.73 (d, $J = 7.0$ Hz, 1H), 7.63–7.57 (m, 11H), 7.47–7.35 (m, 9H), 2.03–1.97 (m, 4H), 0.38–0.36 (t, $J = 7.0$ Hz, 6H); ^{13}C-NMR (75 MHz, $CDCl_3$, δ): 192.8, 151.6, 149.6, 1428, 142.6, 141.6, 139.2, 137.2, 136.7, 135.6, 134.8, 133.4, 133.1, 131.1, 129.9, 129.7, 129.0, 128.3, 128.1, 126.4, 121.8, 120.7, 119.7, 56.5, 32.9, 8.9; IR (KBr): 3015, 2970, 1738, 1703, 1427, 1366, 1228, 1216, 1140, 1085, 681 cm^{-1}; FABMS (*m/z*): 584 [M^+]; HRMS (FAB, *m/z*): [M^+] calcd for $C_{42}H_{36}OSi$, 584.2535; found, 584.2525.

(9,9-Diethyl-7-(4,4,5,5-tetramethyl-1,3,2-dioxaborolan-2-yl)-9H-fluoren-2-yl)triphenyl-silane (24): **24**was prepared by the same procedure as for **13**, from (7-bromo-9,9-diethyl-9H-fluoren-2-yl)triphenylsilane (1.50 g, 1.92 mmol). Yield: 1.15 g, 70%. ^{1}H-NMR (300 MHz, $CDCl_3$, δ): 7.82–7.71 (m, 3H), 7.58 (t, $J = 6.5$ Hz, 4H), 7.53–7.42 (m, 9H), 7.40 (d, $J = 7.2$ Hz, 5H), 1.99–1.95 (m, 4H), 1.27 (s, 12H), 0.30 (t, $J = 7.3$ Hz, 6H); ^{13}C-NMR (75 MHz, $CDCl_3$, δ): 149.9, 149.8, 144.5, 143.1, 136.7, 135.9, 135.4, 134.8, 134.0, 133.3, 131.2, 129.8, 129.6, 129.3, 128.1, 119.9, 119.6, 84.0, 56.4, 32.7, 25.2, 8.8; IR (KBr): 2978, 1461, 1427, 1143, 1109, 1075, 860, 821, 701 cm^{-1}; FABMS (*m/z*): 606 [M^+]; HRMS (FAB, *m/z*): [M^+] calcd for $C_{41}H_{43}BO_2Si$, 606.3125; found, 606.3129.

3,5-bis(9,9-Diethyl-7-(triphenylsilyl)-9H-fluoren-2-yl)benzaldehyde (25): **25** was prepared by the same procedure as for **7**, from (9,9-diethyl-7-(4,4,5,5-tetramethyl-1,3,2-dioxaborolan-2-yl)-9*H*-fluoren-2-yl)triphenylsilane (1.06 mg, 1.75 mmol) and 3,5-dibromobenzaldehyde (210 mg, 0.79 mmol. Yield: 630 mg, 75%. ^{1}H-NMR (300 MHz, $CDCl_3$, δ): 10.21 (s, 1H), 8.16 (d, $J = 8.2$ Hz, 2H), 7.84 (d, $J = 8.8$ Hz, 2H), 7.75 (d, $J = 8.2$ Hz, 2H), 7.73 (d, $J = 7.0$ Hz, 2H), 7.71–7.52 (m, 17H), 7.48–7.36 (m, 19H), 2.17–1.97 (m, 8H), 0.41–0.32 (m, 12H); ^{13}C-NMR (75 MHz, $CDCl_3$, δ): 192.9, 151.7, 149.6, 143.5, 142.6, 141.7, 139.4, 137.7, 136.7, 135.6, 134.8, 133.2, 132.3, 131.1, 129.9, 128.2, 127.4, 126.6, 122.0, 120.8, 119.7, 56.6, 32.9, 8.9; IR (KBr): 3016, 2970, 1738, 1366, 1228, 1216, 1108, 699 cm^{-1}; FABMS (*m/z*): 1063 [$M^+ + H$]; HRMS (FAB, *m/z*): [$M^+ + H$] calcd for $C_{77}H_{67}OSi_2$, 1063.4730; found, 1063.4733.

4′,4″-(Diphenylsilanediyl)dibiphenyl-4-carbaldehyde (26): **26** was prepared by the same procedure as for **21**, from *bis*(4-bromophenyl)diphenylsilane (600 mg, 1.21 mmol) and 4-formylphenylboronic acid (455 mg, 3.03 mmol). Yield: 350 mg, 53%. ^{1}H-NMR (300 MHz, $CDCl_3$, δ): 10.07 (s, 2H), 7.97 (d, $J = 8.2$ Hz, 4H), 7.79 (d, $J = 7.0$ Hz, 4H), 7.70 (d, $J = 7.0$ Hz, 6H), 7.66–7.62 (m, 6H), 7.49–7.40 (m, 6H); ^{13}C-NMR (75 MHz, $CDCl_3$, δ): 152.8, 151.6, 149.1, 148.4, 142.8, 142.4, 140.8, 138.1, 137.6, 136.6, 135.3, 130.8, 130.7, 130.3, 129.1, 128.5, 128.2, 128.0, 127.4, 127.1, 125.0, 124.8, 123.6, 121.7, 121.5, 120.4, 57.2, 33.9, 9.7; IR (KBr): 3016, 2970, 1738, 1366, 1227, 1216, 111, 811, 739 cm^{-1}; FABMS (*m/z*): 545 [$M^+ + H$]; HRMS (FAB, *m/z*): [$M^+ + H$] calcd for $C_{38}H_{29}O_2Si$, 545.1937; found, 545.1940.

7-(Diphenylamino)-9,9-diethylfluorene-2-carbaldehyde (27): Compound **27** was synthesized similarly to compound **18** and obtained (0.820 g) at a yield of 92%. ^{1}H-NMR (300 MHz, $CDCl_3$, δ): 10.02 (s, 1H), 7.84–7.81 (m, 2H), 7.72 (d, $J = 8.6$ Hz, 1H), 7.62 (d, $J = 8.1$ Hz, 1H), 7.32–7.24 (m, 4H), 7.15–7.02 (m, 8H), 2.07–1.84 (m, 4H), 0.35 (t, $J = 7.3$ Hz, 6H); ^{13}C-NMR ($CDCl_3$, 125 MHz, δ): 192.5, 153.1, 150.8, 149.2, 148.2, 147.9, 134.8, 134.6, 131.1, 129.6, 124.7, 123.4, 123.2, 121.9, 119.4, 118.4, 56.4, 32.7, 8.8; FT-IR (KBr): 3035, 2962, 2851, 2728, 1691, 1593, 1490, 1461, 1344, 1279, 1168, 754, 697 cm^{-1}; EIMS (*m/z*): 417 [M^+]; HRMS (EI, *m/z*): [M^+] calcd for $C_{30}H_{27}NO$, 417.2093; found, 417.2093.

(7-(Diphenylamino)-9,9-diethylfluoren-2-yl)methanol (28): Ethanol was added to a mixture of **27** (245 mg, 0.58 mmol) and sodium borohydride (89.0 mg, 2.35 mmol) in a 2-neck, round-bottomed flask, refluxed at 78 °C for 2 h, and the reaction mixture poured into ice water, extracted with diethyl ether, and washed with water. The combined organic layers were dried with anhydrous $MgSO_4$, filtered, evaporated to dryness, and the crude product purified by silica gel column chromatography using ethyl acetate/hexane (1:5 v/v) to produce a white solid (243 mg, 99% yield). ^{1}H-NMR (300 MHz, $CDCl_3$, δ): 7.59 (d, $J = 8.1$ Hz, 1H), 7.55 (d, $J = 8.2$ Hz, 1H), 7.30–7.21 (m, 6H), 7.12 (dd, $J = 8.7$, 1.3 Hz, 4H), 7.05–6.97 (m, 4H), 4.74 (s, 2H), 1.94–1.89 (m, 4H), 1.77 (s, 1H), 0.34 (t, $J = 7.3$ Hz, 6H); ^{13}C-NMR (75 MHz, $CDCl_3$, δ): 151.7, 150.6, 148.3, 147.4, 141.2, 139.3, 136.6, 129.4, 126.2, 124.0, 123.9, 122.7, 121.8, 120.6, 119.7, 119.3, 66.1, 56.3, 32.9, 8.8; FT-IR (ATR): 3361, 3036, 2959, 2929, 2874, 1588, 1492, 1469, 1454, 1329, 1302, 1274, 1030, 1014, 889, 820, 744, 690, 669 cm^{-1}; EIMS (*m/z*): 419 [M^+]; HRMS (EI, *m/z*): [M^+] calcd for $C_{30}H_{29}NO$, 419.2249; found, 419.2247.

(7-(Diphenylamino)-9,9-diethylfluoren-2-yl)methylphosphonate (29): Triethylphosphite (5.0 mL, excess) was added to **28** (245 mg, 0.584 mmol) and charged with nitrogen and iodine (148 mg, 0.584 mmol) all at once at 0 °C, stirred for 30 min, warmed up to room temperature, and stirred for 12 h. Excess triethylphosphite was removed by distillation, the residue extracted with ethyl acetate, washed with water and the combined organic layers dried with anhydrous $MgSO_4$, filtered, and evaporated to dryness. The crude product was purified by silica gel column chromatography using ethyl acetate to produce yellow oil (260 mg, 83% yield). ^{1}H-NMR (300 MHz, $CDCl_3$, δ): 7.56 (d, $J = 7.5$ Hz, 1H), 7.54 (d, $J = 8.1$ Hz, 1H), 7.27–7.22 (m, 6H), 7.11 (dd, $J = 7.9$, 2.2 Hz, 4H), 7.04–6.97 (m, 4H), 4.03–3.97 (m, 4H), 3.27 (s, 1H), 3.19 (s, 1H), 1.94–1.88 (m, 4H), 1.23 (t, $J = 7.1$ Hz, 6H), 0.34 (t, $J = 7.3$ Hz, 6H); ^{13}C-NMR (75 MHz, $CDCl_3$, δ): 151.5, 150.4 (d, $J_{pc} = 3.3$ Hz), 148.3, 147.3, 140.4 (d, $J_{pc} = 3.3$ Hz), 136.6, 129.7 (d, $J_{pc} = 9.4$ Hz), 129.4, 128.9, 128.8, 124.5 (d, $J_{pc} = 6.6$ Hz), 124.0, 122.7, 120.5, 119.7, 119.4 (d, $J_{pc} = 3.3$ Hz), 62.4 (d, $J_{pc} = 6.6$ Hz), 56.2, 34.3 (d, $J_{pc} = 137.7$ Hz), 32.9, 16.6 (d, $J_{pc} = 6.1$ Hz), 8.8; FT-IR (ATR): 2965, 2910, 1738, 1588, 1493, 1468, 1274, 1249, 1053, 1027, 963, 843, 823, 754, 697 cm^{-1}; EIMS (*m/z*): 539 [M^+]; HRMS (EI, *m/z*): [M^+] calcd for $C_{34}H_{38}O_3NP$, 539.2589; found, 539.2589.

Physical Measurements: The UV-Vis absorption and PL spectra of the newly designed blue dopant materials were measured in dichloromethane (10^{-5} M) using a Scinco S-3100 and Aminco Bowman series 2 luminescence spectrometer. The fluorescent quantum yield was determined in the dichloromethane solution at 293 K against BDAVBi as a reference ($\Phi = 0.86$).[13] Differential scanning calorimetry was performed using a Mettler Toledo DSC 822 instrument operated at heating and cooling rates of 10 and 30 °C min^{-1}, respectively. The ionization potentials (or HOMO energy levels) of the compounds were determined by low energy, photo-electron spectrometry (Riken-Keiki AC-2). LUMO energy levels were estimated by subtracting the energy gap (ΔE_g) from the HOMO energy levels. ΔE_g was determined by the on-set absorption energy from the absorption spectra of the materials. Surface morphology of the film was analyzed with non-contact mode AFM (XE100, PSIA Co.).

OLED Fabrication and Measurement: A device configuration for the blue device was ITO (150 nm)/DNTPD (60 nm)/NPB (30 nm)/MADN:dopant (30 nm)/Alq_3 (20 nm)/LiF(1.0 nm)/Al(200 nm). DNTPD and NPB were hole-injection and hole-transport materials, respectively. Alq_3 was used as an electron transport layer and LiF/Al as the cathode. All organic materials, except for dopants, were deposited at a rate of 1.0 Å s^{-1}. *I–V–L* characteristics and EL spectra of the devices were measured with a Keithley 2400 source measurement unit and a CS 1000A spectrophotometer. The lifetime of the blue devices was measured at a constant luminance of 1 000 cd m^{-2}.

Acknowledgements

S. S. Y. acknowledges the financial support by the Basic Science Research Program through the NRF funded by the Ministry of Education, Science, and Technology (20090073679). J. Y. L. (Sungkyunkwan University) acknowledges the financial support by the NRF (grant No. R11-2007-012-03002-0). J. Y. L. (Dankook University) acknowledges the financial support by the GRRC program of Gyeonggi province (GRRC Dankook 2009-B01, Materials development for high efficiency organic solid state lighting), MKE/ITEP (10028439-2008-21), and a grant (M2009010025) from the Fundamental R&D Program for Core Technology of Materials funded by the MKE.

Received: October 8, 2009
Revised: January 15, 2010
Published online: March 31, 2010

[1] C. W. Tang, S. A. Vanslyke, C. H. Chen, *J. Appl. Phys.* **1989**, *65*, 3610.
[2] C. H. Chen, J. Shi, C. W. Tang, *Coord. Chem. Rev.* **1998**, *171*, 161.
[3] U. Mitschke, P. Bauerle, *J. Mater. Chem.* **2000**, *10*, 1047.
[4] C. W. Tang, S. A. Vanslyke, *Appl. Phys. Lett.* **1987**, *51*, 913.
[5] B. C. Krummacher, V. E. Choong, M. K. Mathsi, S. A. Choulis, F. Jermann, T. Fiedler, M. Zachau, *Appl. Phys. Lett.* **2006**, *88*, 113506.
[6] M. T. Lee, C. H. Liao, C. H. Tasi, C. H. Chen, *Adv. Mater.* **2005**, *17*, 2493.
[7] Y. Li, M. K. Fung, Z. Xie, S. T. Lee, L. S. Hung, J. Shi, *Adv. Mater.* **2002**, *14*, 1317.
[8] C. C. Wu, Y. T. Lin, K. T. Wong, R. T. Chen, Y. Y. Chen, *Adv. Mater.* **2004**, *16*, 61.
[9] L. M. Leung, W. Y. Lo, S. K. So, K. M. Lee, W. K. Choi, *J. Am. Chem. Soc.* **2000**, *122*, 5640.
[10] L. H. Chan, R. H. Lee, C. F. Hsieh, H. C. Yeh, C. T. Chen, *J. Am, Chem. Soc.* **2002**, *124*, 6469.
[11] R. C. Chiechi, R. J. Tseng, F. Marchioni, Y. Yang, F. Wudl, *Adv. Mater.* **2006**, *18*, 325.
[12] C. J. Tonzola, A. P. Kulkarni, A. P. Gifford, W. Kaminsky, S. A. Jenekhe, *Adv. Funct. Mater.* **2007**, *17*, 863.
[13] C. L. Li, S. J. Shieh, S. C. Lin, R. S. Liu, *Org. Lett.* **2003**, *5*, 1131.
[14] M.-T. Lee, C.-H. Liao, C.-H. Tsai, C. H. Chen, *Adv. Mater.* **2005**, *17*, 2493.
[15] S. J. Lee, J. S. Park, K.-J. Yoon, Y.-I. Kim, S.-H. Jin, S. K. Kang, Y.-S. Gal, S. Kang, J. Y. Lee, J.-W. Kang, S.-H. Lee, H.-D. Park, J.-J. Kim, *Adv. Funct. Mater.* **2008**, *18*, 3922.
[16] Y.-Y. Lyu, J. Kwak, O. Kwon, S.-H. Lee, D. Kim, C. Lee, K. Char, *Adv. Mater.* **2008**, *20*, 2720.
[17] M. J. Frisch, G. W. Trucks, H. B. Schlegel, G. E. Scuseria, M. A. Robb, J. R. Cheeseman, J. A. Montgomery, T. Vreven, Jr, K. N. Kudin, J. C. Burant, J. M. Millam, S. S. Iyengar, J. Tomasi, V. Barone, B. Mennucci, M. Cossi, G. Scalmani, N. Rega, G. A. Petersson, H. Nakatsuji, M. Hada, M. Ehara, K. Toyota, R. Fukuda, J. Hasegawa, M. Ishida, T. Nakajima, Y. Honda, O. Kitao, H. Nakai, M. Klene, X. Li, J. E. Knox, H. P. Hratchian, J. B. Cross, C. Adamo, J. Jaramillo, R. Gomperts, R. E. Stratmann, O. Yazyev, A. J. Austin, R. Cammi, C. Pomelli, J. W. Ochterski, P. Y. Ayala, K. Morokuma, G. A. Voth, P. Salvador, J. J. Dannenberg, V. G. Zakrzewski, S. Dapprich, A. D. Daniels, M. C. Strain, O. Farkas, D. K. Malick, A. D. Rabuck, K. Raghavachari, J. B. Foresman, J. V. Ortiz, Q. Cui, A. G. Baboul, S. Clifford, J. Cioslowski, B. B. Stefanov, G. Liu, A. Liashenko, P. Piskorz, I. Komaromi, R. L. Martin, D. J. Fox, T. Keith, M. A. Al-Laham, C. Y. Peng, A. Nanayakkara, M. Challacombe, P. M. W. Gill, B. Johnson, W. Chen, M. W. Wong, C. Gonzalez, J. A. Pople, Gaussian 03, revision B05, Gaussian, Inc, Pittsburgh, PA **2003**.
[18] Y. Cao, I. D. Parker, G. Yu, C. Zhang, A. J. Heeger, *Nature* **1999**, *397*, 414.
[19] D. Beljonne, A. Ye, Z. Shuai, J.-L. Brédas, *Adv. Funct. Mater.* **2004**, *14*, 684.
[20] H. Y. Chen, W. Y. Lam, J. D. Luo, Y. L. Ho, B. Z. Tang, D. B. Zhu, M. Wong, H. S. Kwok, *Appl. Phys. Lett.* **2002**, *81*, 574.
[21] G. S. He, L. Yuan, F. Xu, P. N. Prased, B. A. Reinhardt, J. W. Baur, R. A. Vaia, L.-S. Tan, *Chem. Mater.* **2001**, *13*, 1896.
[22] J.-W. Kang, D.-S. Lee, H.-D. Park, Y.-S. Park, J. W. Kim, W.-I. Jeong, K.-M. Yoo, K. Go, S.-H. Kim, J.-J. Kim, *J. Mater. Chem.* **2007**, *17*, 3714.
[23] K. R. Thomas, J. T. Lin, C. P. Chang, C. H. Chuen, C. C. Cheng, *J. Chin. Chem. Soc (Taipei, Taiwan)* **2002**, *49*, 833.
[24] H. C. Lin, K. W. Lee, C. M. Tsai, K. H. Wei, *Macromolecules* **2006**, *39*, 3808.
[25] X.-H. Zhou, Y.-H. Niu, F. Huang, M. S. Liu, A. K.-Y. Jen, *Marcromolecules* **2007**, *40*, 3015.
[26] R. Kannan, G. S. He, L. Yuan, F. Xu, P. N. Prasad, A. G. Dombroskie, B. A. Reinhardt, J. W. Baur, R. A. Vaia, L. S. Tan, *Chem. Mater.* **2001**, *13*, 1896.